

Opposite Changes in Monsoon Precipitation and Low Pressure System Frequency in Response to Orographic Forcing^❶

TRESA MARY THOMAS^❷,^a GOVINDASAMY BALA,^{a,b} SRINIVAS VENKATA VEMAVARAPU,^{a,c} AND WILLIAM R. BOOS^d

^a Interdisciplinary Centre for Water Research, Indian Institute of Science, Bangalore, India

^b Centre for Atmospheric and Oceanic Sciences, Indian Institute of Science, Bangalore, India

^c Civil Engineering, Indian Institute of Science, Bangalore, India

^d Department of Earth and Planetary Science, University of California, Berkeley, Berkeley, California

(Manuscript received 30 June 2022, in final form 5 May 2023, accepted 30 May 2023)

ABSTRACT: Monsoon low pressure systems (LPS) are synoptic-scale disturbances that form along the quasi-stationary trough of the larger-scale South Asian summer monsoon, producing a large fraction of total monsoon precipitation. Here, we use an Earth system model to investigate the influence of Tibetan and Himalayan orography (THO) on mean monsoon strength and LPS activity. The influence of THO height on LPS activity has not been investigated before. The model simulates decreased mean monsoon circulation and precipitation when THO is removed, but the number of LPS and the meridional extent of LPS activity increase; this is an unexpected, important finding given that LPS are principal rain-bearing systems of the monsoon. The decreased mean monsoon circulation and precipitation on removal of THO are attributed to enhanced mixing of dry extratropical air into the humid monsoon domain, as demonstrated by prior studies. The increase in LPS frequency and the meridional extent of LPS activity is attributed to the increase in magnitude and meridional extent of the low-level meridional shear of zonal wind, which previous work showed amplifies LPS through barotropic growth. Specifically, as monsoon precipitation decreases, the sensible heat-driven low-level trough intensifies and shifts equatorward; this strengthens the shear zone in which LPS grow. Conversely, increasing THO height decreases the magnitude and meridional extent of cyclonic shear over India, decreasing LPS frequency and the spatial extent of LPS activity while increasing total monsoon precipitation. These results demonstrate that LPS activity and total monsoon rainfall can undergo large, opposing changes in response to imposed forcings.

SIGNIFICANCE STATEMENT: Monsoon low pressure systems (LPS) are propagating atmospheric vortices that deliver a large fraction of seasonal-mean precipitation to agricultural regions of India. The influence of Tibetan and Himalayan orography (THO) on the South Asian monsoon is an active area of research, but its effect on LPS has remained unexplored. Here, a global climate model is used to simulate LPS characteristics for different heights of THO. Flattening the THO reduces total summer monsoon precipitation but increases the number of LPS and the spatial extent of LPS activity. We attribute these LPS changes to a decrease in the magnitude and meridional extent of the hydrodynamically unstable low-level cyclonic shear zone over South Asia that occurs when orography is flattened.

KEYWORDS: Barotropic flows; Orographic effects; Wind shear; Monsoons

1. Introduction

Synoptic-scale cyclonic disturbances called monsoon low pressure systems (LPS) form over the Indian subcontinent during the summer monsoon season (June–September; Mooley and Shukla 1987). About half of these are stronger systems called depressions and deep depressions, while the other half are weaker systems called lows (IMD 2021). Most LPS form over the warm surface waters of the north Bay of Bengal (BoB) and move in the west or northwest direction along the monsoon trough, producing a large fraction of the total summer precipitation over continental South Asia (Sikka 1977; Goswami 1987;

Yoon and Chen 2005; Hurley and Boos 2015). South Asian monsoon precipitation is also known to be highly sensitive to the distribution of orography, with the Himalayas and adjacent mountains and plateaus producing a monsoon that is stronger and located further poleward than any other monsoon on Earth (Hahn and Manabe 1975; Chakraborty et al. 2006; Wu et al. 2018; Boos and Kuang 2010).

Early studies (Sikka 1977; Keshavamurty et al. 1978) suggested that monsoon LPS may grow through barotropic instability, baroclinic instability, and various mechanisms of coupling with moist convection. Goswami (1987) suggested that LPS are Rossby–gravity waves that propagate northwestward as cumulus convection couples with the maxima of low-level cyclonic vorticity. Recently, Diaz and Boos (2019a,b) argued that monsoon depressions are a type of moist barotropic instability, which draws energy from the meridionally sheared basic state with some interaction with precipitating ascent. Meridional gradients in moisture have also been argued to foster LPS growth (Adames and Ming 2018); both barotropic growth and amplification by convective coupling in the presence of a moisture gradient have

^❶ Supplemental information related to this paper is available at the Journals Online website: <https://doi.org/10.1175/JCLI-D-22-0476.s1>.

Corresponding author: Tresa Mary Thomas, tresathomas@iisc.ac.in

been shown to amplify LPS-like vortices in an idealized cloud-resolving model (Diaz and Boos 2021). Mishra (2021) has also found that the necessary condition for barotropic instability is satisfied in monsoon depression formation.

Many studies (Hahn and Manabe 1975; Chakraborty et al. 2002, 2006; Zhang et al. 2015) have investigated the influence of various orographic barriers on the Indian monsoon circulation and precipitation. Boos and Kuang (2010) found that South Asian summer monsoon circulation is unaffected by the removal of the Tibetan Plateau, with only the presence of a narrow orography of the Himalayas and adjacent mountain ranges south of the Plateau required to produce a strong monsoon by insulating continental India from the dry extratropics (see also Chakraborty et al. 2006). Other studies (Park et al. 2012; Wu et al. 2012) suggest that the enhanced monsoon strength over India in the presence of the Himalayan orography is governed by surface heating and the ensuing sensible heat fluxes during the premonsoon season. However, Nie et al. (2010) and Boos and Kuang (2013) show that the south Asian summer monsoon system is in convective quasi equilibrium and suggest that local moist energy sources and the suppression of dry intrusions by orography maintain high subcloud-layer moist entropy over continental India and thereby the strong monsoon circulation. In contrast, He (2017) suggests the surface sensible heating is important for monsoon strength, producing a positive feedback between moist convection over the south slope of the Himalayas and the large-scale circulation when the height of the Himalayas is increased. Ashfaq (2020) takes a middle ground and concludes that sensible heating over Tibet might be only one of the many processes that enhance the meridional tropospheric temperature gradient (MTG) and precipitation over India, while the Himalayas and adjacent mountain ranges act as both a barrier and modulator of dynamic and thermodynamic characteristics of the summer monsoon.

Regardless of the mechanism by which orography alters monsoon strength, all previous studies of the influence of Tibetan and Himalayan orography (THO) on the South Asian monsoon agree that a late monsoon onset, a southward shift in the location of the monsoon trough, and reduced summer monsoon precipitation result from the removal of the orography. As monsoon LPS are a major contributor to monsoon precipitation (Thomas et al. 2021) and as LPS propagate along the monsoon trough axis (Sikka 1977; Goswami 1987), substantial changes in LPS statistics and characteristics are expected with the change in the height of THO. With THO rising at around 20 mm yr^{-1} (Bettinelli et al. 2006), understanding the effect of the height of THO on LPS characteristics seems crucial for understanding the evolution of South Asian monsoon on paleo time scales. Studies (Kitoh 1997; Okajima and Xie 2007) have also found that air-sea interactions are crucial for determining the orographic effect on monsoons and global climate change. To our knowledge, no previous study has investigated the influence of THO on the number and overall activity of LPS in India. Hunt and Parker (2016) studied the possible influence of Himalayan orography on the propagation of monsoon depressions, but there is a much broader question of how South Asian orography in general affect the number, intensity, and precipitation of monsoon LPS. We address this important research gap in this paper.

2. Model, simulations, and methods

The coupled version of the NCAR Earth system model, the Community Earth System Model (CESM1.2.2), is used in this study. CESM1.2.2 is a fully coupled climate model for simulating Earth's past, present, and future climate states (Hurrell et al. 2013). It is supported by the National Science Foundation (NSF) and is maintained by the Climate and Global Dynamics (CGD) Laboratory at the National Center of Atmospheric Research (NCAR). It has seven geophysical named as follows: atmosphere, ocean, land, river-runoff, sea-ice, land-ice, and ocean-wave. A coupler coordinates these components by passing information between them in a stepwise manner with time. The atmospheric component of CESM1.2.2 is the Community Atmosphere Model version 4 (CAM4; Neale et al. 2013), which is configured here with a $0.9^\circ \times 1.25^\circ$ horizontal resolution and 26 vertical levels for our simulations. Furthermore, the land component of CESM, the Community Land Model version 4 (CLM4; Oleson et al. 2010), is also configured with $0.9^\circ \times 1.25^\circ$ horizontal resolution. CLM4 has representation for carbon and nitrogen biochemistry (Doney et al. 2006). The ocean component is the extension of the parallel ocean program (PoP, version 2; Smith et al. 2010) with approximately 1° horizontal resolution on the displaced pole grid. The Community Ice Code (CICE, version 4; Hunke and Lipscomb 2008) is the sea ice component.

In this study, we have performed the present-day simulations of the fully coupled version of the model (Compset, B_2000_CN). The model is spun up by forcing it with present-day concentrations (corresponding to the year 2000) of greenhouse gases and aerosols. Initial condition files corresponding to the present-day conditions are provided by existing present-day simulations at NCAR. Four present-day experiments are performed using the model: the first is a control simulation (M1.0) with the current height of THO, and in the other experiments (M0.0, M0.5, and M1.5), the height of THO is altered by 0, 0.5, and 1.5 times its present value, respectively. It is achieved by setting three variables, namely, PHIS (surface geopotential), SGH (standard deviation of surface elevation), and SGH30 (surface roughness) in the USGS Topography file of the model to 0, 0.5, and 1.5 times the default value (boundary condition provided by NCAR) inside the rectangular area between $60^\circ\text{--}120^\circ\text{E}$ and $25.9^\circ\text{--}43.8^\circ\text{N}$ (Fig. 1). To avoid a sharp change in orography along the boundaries of the chosen rectangular area, the above variables are smoothed along the boundaries outside of the rectangular area, where they are interconnected to other mountain ranges, i.e., between $43.8^\circ\text{--}48.5^\circ\text{N}$ and $21.2^\circ\text{--}25.9^\circ\text{N}$ along the longitudinal extent $60^\circ\text{--}120^\circ\text{E}$ and between 53.75° and 60°E along the latitudinal extent $25.9^\circ\text{--}43.8^\circ\text{N}$. The smoothing is achieved by the two-dimensional Gaussian smoothing kernel technique using the MATLAB package. The topographical domain mainly comprises the Tibetan and Himalayan orography and the Karakoram, Hindu Kush, and Pamir-Alay ranges, and Kunlun, Tianshan, and Qilian Shan mountains. The area is bounded by the Iranian plateau toward the west, the Gobi Desert and other mountain ranges in the north, and the southeast Asian mountains in the southeast.

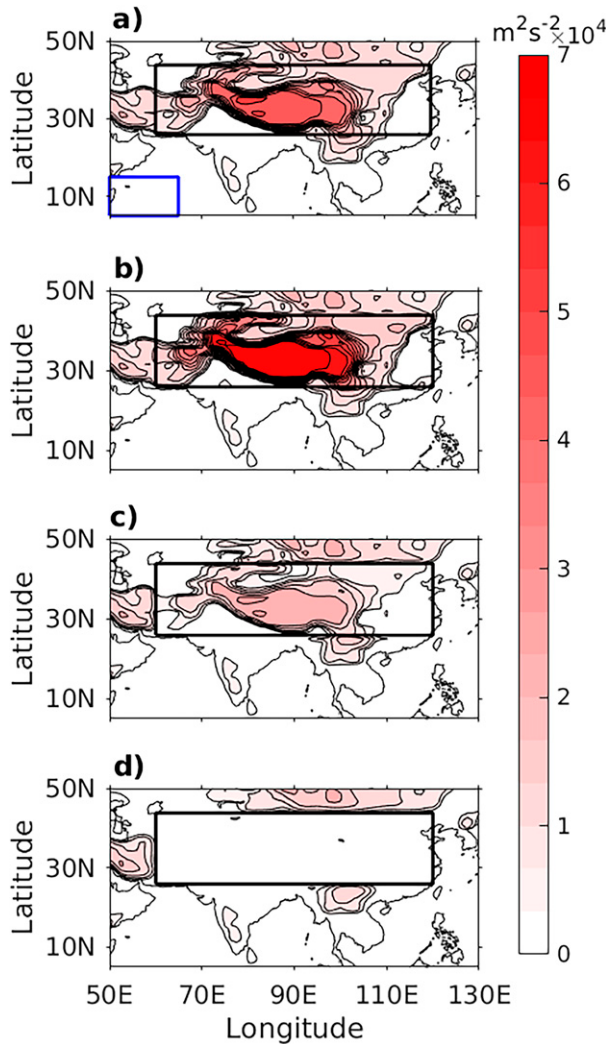


FIG. 1. Surface geopotential height ($\text{m}^2 \text{ s}^{-2}$) in the (a) M1.0, (b) M1.5, (c) M0.5 and (d) M0.0 simulations. The actual topography over the rectangular domain bounded by 60° – 120°E and 25.9° – 43.8°N (shown as a black box in the panels) is multiplied by 1.0, 1.5, 0.5, and 0 in the M1.0, M1.5, M0.5, and M0.0 simulations, respectively. The blue box in (a) corresponds to the domain used for calculation of the kinetic energy of the low-level jet, which is shown in Fig. 2b.

The spinup period to reach near-equilibrium conditions for the present-day control simulation is 197 years. Using this equilibrium state as the initial condition, branch runs were performed with altered orography. The length of the runs depended on the time required for the model to reach near equilibrium conditions with altered orography, in terms of the variables described below. The model runs with 0.5 and 1.5 times altered orography reached equilibrium within 8 years (i.e., by 205 years). After reaching equilibrium, the model is run for 37 years with data output at 6-hourly intervals. The 37-yr simulations are referred to as M0.5 and M1.5 respectively. The model run without THO required 12 years for reaching equilibrium (i.e., by 209 years). The 37-yr simulation (with data output at 6-hourly interval) after

reaching equilibrium is referred to as M0.0. The plots of global mean surface temperature, the net radiative flux at the top of the model, and surface albedo (Fig. S1 in the online supplemental material) during the spinup and analysis period for the experiments indicate that the model has reached near equilibrium. However, the nonzero value of the net radiative flux at the top of the model (Fig. S1) indicates that the deep ocean has not reached equilibrium.

LPS are tracked in the simulations considering the automated tracking algorithm using geopotential criteria (ATAGC; Thomas et al. 2021, 2022). A brief description of ATAGC is provided in the supplemental material (Text S1). The changes in LPS characteristics and statistics on altering the height of THO are evaluated.

3. Results and discussion

The ability of CESM to simulate the known features of monsoon and LPS characteristics in present-day control simulations (M1.0) has been extensively assessed in an earlier study (Thomas et al. 2022). We briefly discuss the key results of the model evaluation pertaining to monsoon circulation and LPS here. CESM can simulate the general monsoon features such as seasonality, northward propagation of monsoon precipitation, and mean monsoon winds. However, the annual mean precipitation simulated by CESM ($96.4 \pm 7.5 \text{ cm}$) during a 37-yr period over India exceeds the corresponding estimate ($82.9 \pm 7.7 \text{ cm}$) based on IMD (India Meteorological Department) observations over 1979–2015 by 16%. Similar to earlier studies (Hanf and Annamalai 2020; Yao et al. 2016) that used CAM4/5, M1.0 also simulates a wet bias in mean monsoon precipitation over the northern, southern, and western parts of India and a dry bias is simulated over the eastern part. Hanf and Annamalai (2020) attribute these biases to an unrealistic representation of boundary layer processes off the coast of Somalia. Furthermore, the statistical features of LPS simulated by CESM (Thomas et al. 2022) closely resemble features of LPS tracked from ERA-Interim data (Thomas et al. 2021), except for a southward latitudinal shift ($\sim 4^\circ$) in the spatial pattern of LPS characteristics (genesis and track density) and the associated precipitation in the case of CESM simulation. The southward latitudinal shift is associated with the southward latitudinal shift of the monsoon trough which is related to a smaller midtropospheric meridional temperature gradient (MTG) magnitude simulated in the CTRL simulation (compared to ERA-Interim) during both the premonsoon and monsoon periods (Thomas et al. 2022).

In this paper, as discussed in section 1, we focus on the influence of THO on the LPS characteristics, as this was not the focus of past studies that primarily investigated the influence of THO on broader monsoonal circulation and precipitation. To demonstrate that our results are consistent with the past studies, a detailed analysis of the effect of THO on mean monsoon circulation and precipitation over India is first provided.

a. Effect on mean monsoon behavior

1) SUMMER MONSOON ONSET

Using the atmospheric general circulation model of the National Meteorological Centre at T-80 resolution ($\sim 1.411^\circ$),

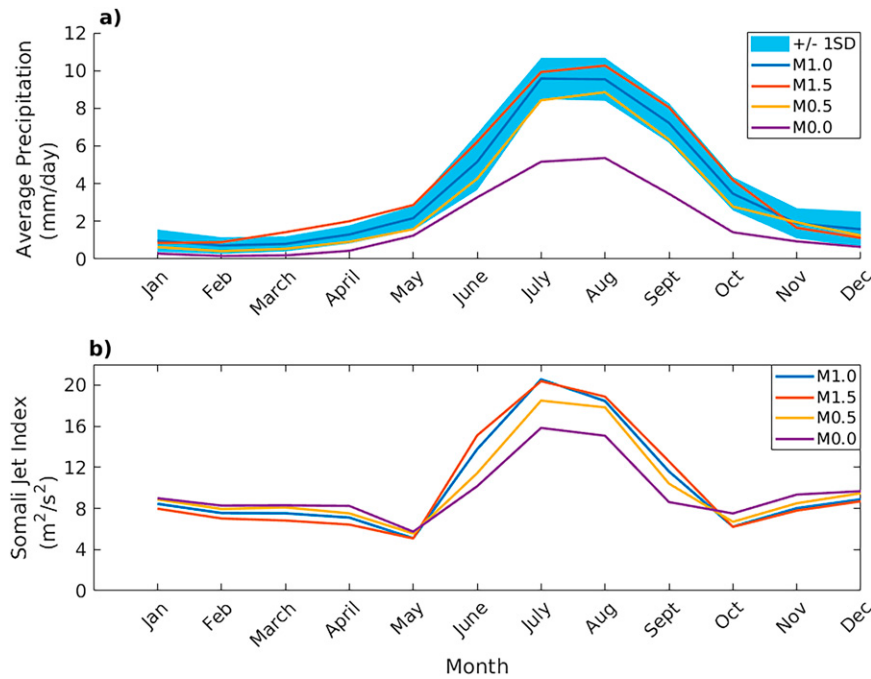


FIG. 2. (a) The seasonal precipitation cycle over India in the CESM M1.0, M1.5, M0.5, and M0.0 simulations. The monthly means of precipitation are calculated over a 37-yr period. The blue shading shows the uncertainty in the case of M1.0 estimated as ± 1 standard deviation of monthly mean precipitation. (b) Climatological monthly mean kinetic energy of the low-level jet, calculated as kinetic energy of winds at 850 hPa averaged over 50° – 65° E and 5° – 15° N in CESM simulations over a 37-yr period. The domain used for the kinetic energy calculation is shown in Fig. 1a.

Chakraborty et al. (2002) simulated a delay in monsoon onset by around 39 days over India for the year 1998 when the topography over the whole world is removed. Following the same study, we consider the monsoon onset day as the first day of the monsoon season when the precipitation is greater than 4 mm day^{-1} for 5 consecutive days over the Indian region (the land area covering 8° – 28.7° N and 67.5° – 91.25° E). We find that the onset is advanced (delayed) when the height of THO is increased (decreased): the onset occurs around 16 June (± 11 days) in the M1.0 simulation, while the onset is advanced by around 3 days (13 June ± 9 days) in M1.5 compared to M1.0. Here the uncertainty is estimated as one standard deviation in the onset date calculated from 37 years of simulations. In contrast, the onset is delayed by 1 day in M0.5 (17 June ± 13 days) and 1 week in M0.0 (23 June ± 16 days) compared to M1.0. Thus, our results are qualitatively in agreement with those of Chakraborty et al. (2002) regarding delay in the onset of monsoon on the removal of THO (in M0.0).

2) MEAN SUMMER MONSOON PRECIPITATION

In agreement with several earlier studies (Chakraborty et al. 2006; Zhang et al. 2015), we find that reducing (increasing) the height of THO causes a reduction (increase) in summer monsoon (June–September) precipitation over India (Fig. 2). A 9.3% increase is simulated in the mean summer monsoon precipitation over India in the M1.5 (105.4 ± 8.4 cm)

simulation compared to M1.0 (96.4 ± 7.5 cm, Table 1). In contrast, a decrease of 11.5% and 44% are simulated in the case of M0.5 (85.3 ± 9.1 cm) and M0.0 (53.8 ± 9.2 cm), respectively. Here the uncertainty is estimated as one standard deviation in mean summer monsoon precipitation over the 37-yr simulation period. The sensitivity of precipitation to the height of the THO is thus not linear and is stronger for lower heights. Investigation of the spatial distribution of mean monsoon precipitation over India in our simulations showed that the major effect of partial reductions in topographic height occurred over the foothills of the Himalayas (Fig. 3). Only complete removal of the THO results in the reduction of monsoon precipitation throughout India, with large decreases simulated along the foothills of the Himalayas and along the monsoon core region, in central India (Fig. 3; Table 1). The intensified precipitation along the southern slope of the Himalayas on increasing the height of THO is consistent with earlier studies (He 2017; Boos and Kuang 2013).

3) MEAN SUMMER MONSOON CIRCULATION AND MTG

Another distinctive feature of the monsoon is the cross-equatorial flow of westerlies that reach the Indian subcontinent. As in earlier studies (Hahn and Manabe 1975; Zhang et al. 2015), cross-equatorial flow during the summer monsoon season is established in all our simulations with different heights of THO (Fig. 4). However, the strength of the monsoon circulation

TABLE 1. Climatological means and LPS-related precipitation characteristics discerned from CESM simulations M1.0, M1.5, M0.5, and M0.0 during the summer monsoon season over a 37-yr period. Precipitation-related quantities and the equivalent potential temperature are averages over India. The mean barotropic shear and second derivative of geopotential height in the meridional direction are estimated over 70°–90°E between 10° and 26°N. The midtropospheric meridional temperature gradient (MTG) is calculated as the difference in temperature between two boxes of latitudinal extent 10°–35°N and 15°S–10°N averaged along the longitudinal belt spanning 30°–110°E, and tropospheric levels between 200 and 700 hPa. The uncertainty is represented by one standard deviation, and an asterisk denotes that the changes in mean precipitation are significant at a 95% confidence level as per the two-sample *t* test.

Characteristics	M1.5	M1.0	M0.5	M0.0
Total precipitation (cm)	$105.4 \pm 8.4^*$	96.4 ± 7.5	$85.3 \pm 9.1^*$	$53.8 \pm 9.2^*$
MTG during premonsoon season (K)	-3.75	-3.9	-4.25	-4.42
MTG during summer monsoon season (K)	2.73	2.18	1.54	0.89
Barotropic shear ($\partial U/\partial y$) (s^{-1})	-0.63	-0.67	-0.71	-0.81
Second derivative of geopotential height at 850 hPa in the meridional direction ($m^2 s^{-2}$ per degree squared)	0.15	0.09	0.24	0.40
Equivalent potential temperature (K)	348.24	348.11	346.39	341.71
Precipitable water ($kg m^{-2}$)	49.1	48.7	48.2	42.3
Precipitation on LPS days ($mm day^{-1}$)	9.81 ± 0.9	9.16 ± 0.7	8.14 ± 1.0	$5.22 \pm 0.9^*$
Precipitation associated with LPS ($mm day^{-1}$)	$10.56 \pm 1.4^*$	10.70 ± 1.0	$10.35 \pm 1.4^*$	$7.67 \pm 1.1^*$
Fraction of precipitation associated with LPS (%)	31	37	44	57
Percentage of extreme precipitation events associated with LPS (%)	38.5	48.0	62.7	85.8
Percentage of extreme precipitation amount associated with LPS (%)	37.8	47.3	63.1	87.0

is found to increase (decrease) when the height of the mountain ranges increases (decreases) (Fig. S2). The kinetic energy of low level winds over Arabian sea is normally used as a measure for the strength of monsoon circulation, and they are found to be correlated to monsoon precipitation (Joseph and Sijkumar 2004). Following Ajayamohan (2007), we calculated the kinetic energy of low level monsoon jet as climatological mean kinetic energy of winds at 850 hPa averaged over 50°–65°E and 5°–15°N. During the summer monsoon period, we find an increase in the kinetic energy when the height of THO is increased (Fig. 2). Furthermore, there is reduction in the strength of circulation over the Arabian sea with a reduction in height of THO (Fig. S2), consistent with reduction in monsoon precipitation (Joseph and Sijkumar 2004). The strength of the Somali jet in the case of the M1.5 simulation is comparable to M1.0, indicating there is no increase in the strength when THO is raised.

4) INTRUSION OF DRY MIDLATITUDE AIR

Boos and Kuang (2010) show that the presence of a narrow Himalayan range south of Tibetan Plateau is sufficient to simulate the Southeast Asian summer monsoon circulation by insulating moist air over India from dry extratropical air. Their study finds that the upper tropospheric temperature is maximum south of the plateau during summer, and the maximum lies directly over the location with the highest near-surface equivalent potential temperature because the monsoon system is in quasi-convective equilibrium. In our M1.0 simulation also, the maximum upper tropospheric temperature during summer (Fig. 5a) is south of the plateau, and it lies directly above large values of equivalent potential temperature at 875 hPa (Fig. 6a, Fig. S5). This is consistent with the convective quasi-equilibrium of the monsoon system over India.

Following Goswami and Xavier (2005), we compute (MTG) as the difference between means of mass weighted climatological temperatures corresponding to two boxes of latitudinal extent 10°–35°N and 15°S–10°N averaged along the longitudinal belt spanning 30°–110°E, and tropospheric levels between 200 and 700 hPa. MTG is negative (positive) during the premonsoon (summer monsoon) season (Table 1) and when the height of THO is increased an increase is simulated in the magnitude of MTG (Table 1). MTG is positive during the summer monsoon season (June–September; Table 1), and the onset of monsoon coincides with the reversal in the sign of MTG (Goswami and Xavier 2005). The simulated MTG values for the monsoon season corresponding to the M1.5, M1.0, M0.5, and M0.0 simulations are 2.73, 2.18, 1.54, and 0.89 K, respectively (Table 1). MTG reverses its sign early in the M1.5 simulation leading to an early onset in M1.5 compared to other simulations (Fig. S3). The MTG strength and the associated vertical shear of mean zonal winds (Fig. S4) are indicators of the strength of the monsoon (Goswami and Xavier 2005). In our simulations, a stronger (weaker) MTG during the summer monsoon season is simulated on increasing (decreasing) the height of THO.

When the height of THO is decreased, a southeastward shift is simulated in the location of the maxima of upper tropospheric temperature (Fig. 5) and equivalent potential temperature at 875 hPa (Fig. 6), indicating that THO enhances monsoon precipitation and MTG by acting as a barrier to prevent mixing of high-entropy warm and moist air over India with low-entropy dry extratropical air. The lower orography just to the west of the Tibetan Plateau (e.g., the Hindu Kush range) allows the intrusion of dry extratropical air into the Indian mainland in the M1.0 simulation, as demonstrated by previous studies (Chakraborty et al. 2006; Boos and Hurley 2013);

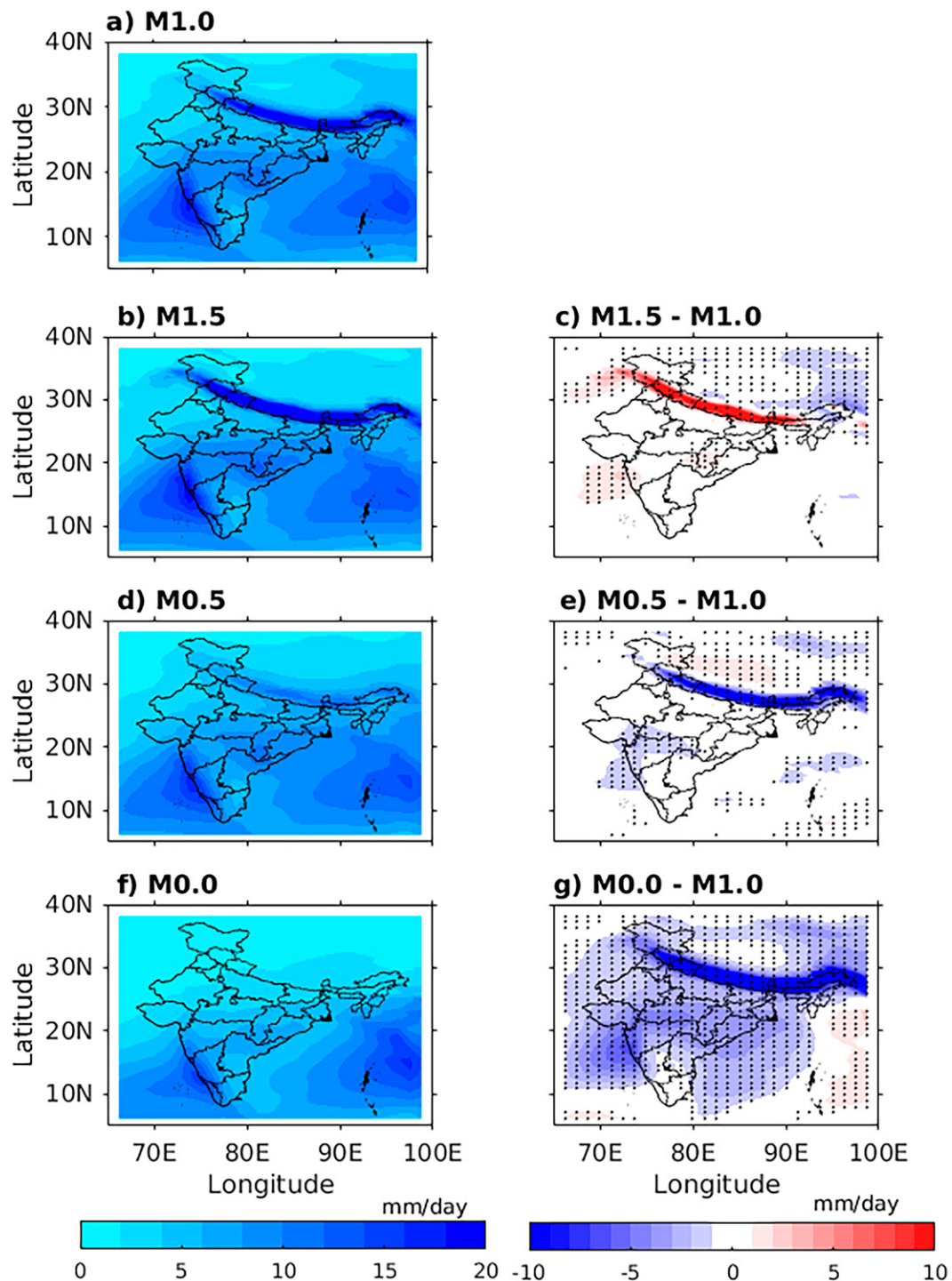


FIG. 3. The mean precipitation over the Indian subcontinent in the summer monsoon season (June–September) in the CESM simulations: (a) M1.0, (b) M1.5, (d) M0.5, and (f) M0.0, and anomalies in the mean precipitation of (c) M1.5, (e) M0.5, and (g) M0.0 simulations relative to M1.0. The means are calculated over a 37-yr period. The hatching in the right panels shows regions where changes in the mean precipitation are significant at a 95% confidence level as per the two-sample t test.

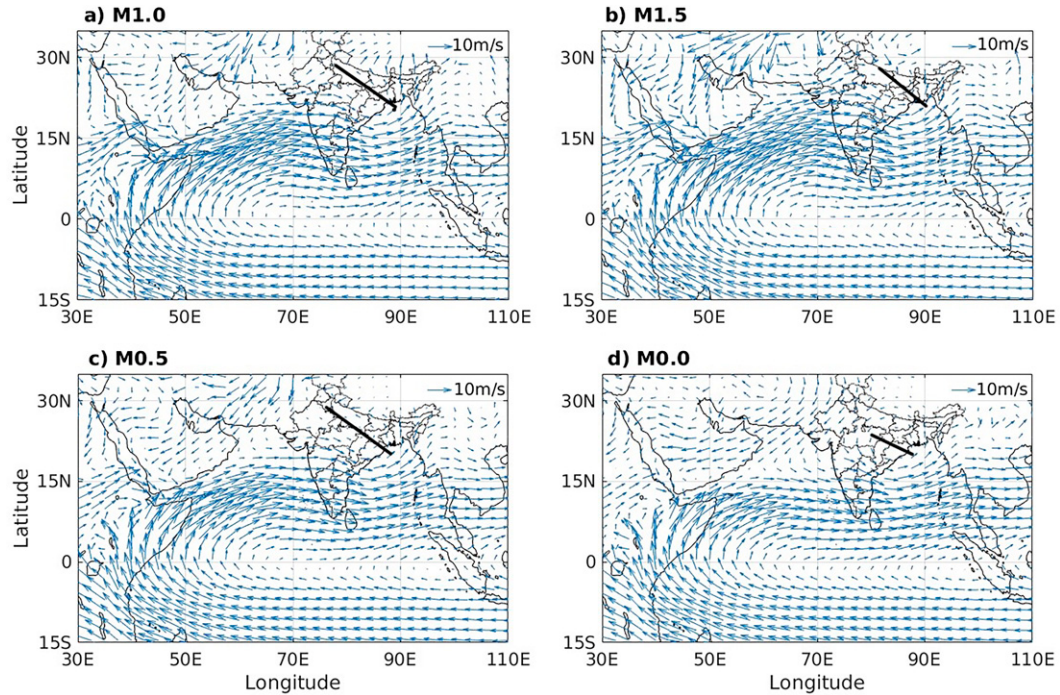


FIG. 4. The climatological mean of the 850-hPa winds (m s^{-1}) during the summer monsoon season (June–September) over the Indian subcontinent in the CESM simulations (a) M1.0, (b) M1.5, (c) M0.5, and (d) M0.0 over a 37-yr period. The black-colored straight line denotes the trough axis, which is constructed by manually connecting locations of zero velocity and extended rightward until the coast.

an increase in orographic heights in that region suppresses those intrusions in the M1.5 simulation. The reduction of topographic heights also reduces the north–south gradient of geopotential height (Figs. 7b,f) over the Arabian Sea. The difference of the average geopotential height between the northern Arabian Sea (15° – 30° N, 50° – 70° E) and southern Arabian Sea (0° – 15° N, 50° – 70° E) decreases as the height of THO decreases ($50.9, 45.1, 31.6$, and $14.1 \text{ m}^2 \text{ s}^{-2}$ for M1.5, M1.0, M0.5, and M0.0, respectively). This in turn leads to a reduction in the magnitude of low-level jet and hence the kinetic energy of the winds over the Arabian Sea (Fig. 2), implying a reduction in monsoon precipitation (Joseph and Sijikumar 2004).

Wu et al. (2012) found that the southeast Asian monsoon is also sensitive to the elevated heating effect of the Himalayas. However, an investigation into the unique effect of surface heating and the consequent increase in transfer of sensible heat to the atmosphere over THO (using experiments with and without sensible heating) on the Indian monsoon is beyond the scope of this study. Such an investigation was performed by Ma et al. (2014), who found that South Asian monsoon strength was most sensitive to surface fluxes south of the Himalayas, in the location of the moist static energy maximum.

b. Effect on LPS characteristics

1) LPS FREQUENCY AND LPS DAYS

Application of the ATAGC algorithm to ERA-Interim reanalysis data identified around 14 LPS per year over the Indian

subcontinent during 1979–2015, which comprised, on average, 8.8 lows, 5.1 depressions, and 0.2 deep depressions (Thomas et al. 2021). Analogous analysis was performed on the CESM simulations. Herein, LPS are categorized based on the geopotential anomaly values (based on eight surrounding grid points) and maximum wind speed at 850 hPa within 5° of the tracked LPS (Table S1). On average, around 13.6 LPS per year are tracked in the M1.0 simulation, which comprised 8 lows, 4.6 depressions, and 1 deep depression (Table 2). This is in close agreement with our earlier study (Thomas et al. 2021) on observed LPS activity over India. Increase (decrease) in the height of THO results in a reduction (an increase) in the frequency of LPS overall, and in the frequency of each category of LPS. Around 12.4 LPS per year comprising 7.3 lows, 4.4 depressions, and 0.7 deep depressions (Table 2) are tracked in the M1.5 simulation, while 16.1 LPS per year consisting of 9.6 lows, 5.5 depressions, and 1 deep depression are tracked in the M0.5 simulation (Table 2). In the M0.0 simulation, the respective numbers further increased to 17.2, 10.2, 5.5, and 1.5 per year (Table 2). On average, LPS are prevalent for about 54.0, 63.0, 71.3, and 81.1 days over India during the monsoon period in the M1.5, M1.0, M0.5, and M0.0 simulations, respectively (Table 2). Similar to mean monsoon precipitation, the increase in the number of LPS and LPS days with the decrease in the height of THO is also nonlinear and is most pronounced when THO is completely removed. The difference in the mean number of all LPS and LPS of different categories in the case of M0.0 compared to M1.0 are found to be significant at 5% significance

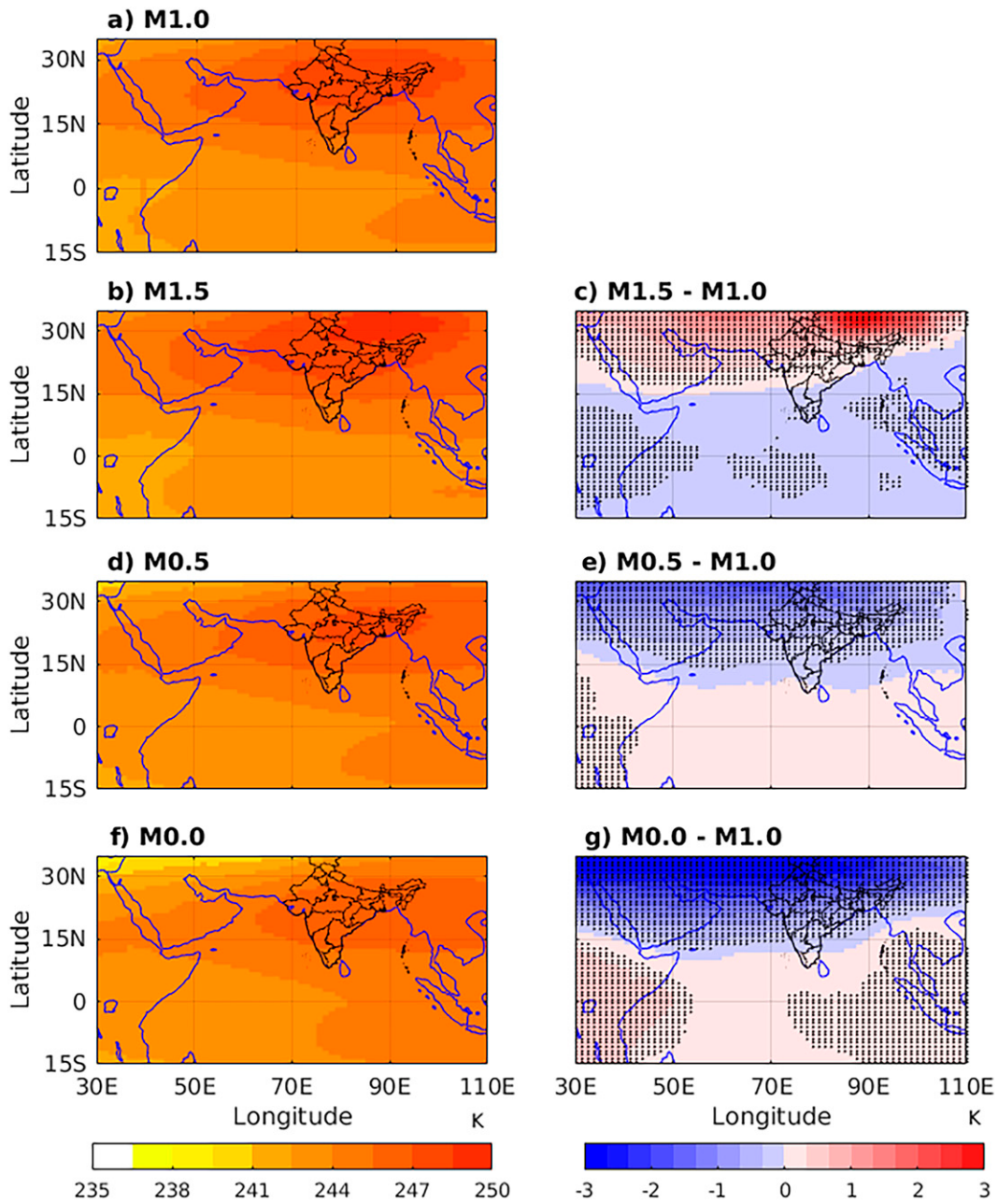


FIG. 5. The mean upper-tropospheric temperature (K) at 300 hPa during the summer monsoon season (June–September) in the CESM simulations (a) M1.0, (b) M1.5, (d) M0.5, and (f) M0.0 over 37-yr periods, and anomalies in the (c) M1.5, (e) M0.5, and (g) M0.0 simulations relative to the M1.0 simulation. The hatching in the right panels shows regions where changes in the mean upper-tropospheric temperature are significant at a 95% confidence level as per the two-sample *t* test.

level (using the two-sample *t* test). To remove the influence of heat lows (which are dry) on our estimation of the frequency of LPS, we also estimated the frequency of LPS that are associated with significant amounts of precipitation (within 1000 km of LPS tracks). We found that the results are unchanged when LPS with small amounts of precipitation are excluded (those with associated precipitation of less than 1, 2, 3, or 5 mm day⁻¹). In summary, we find that the number/frequency of LPS

and their collective duration decrease (increase) when the height of THO is increased (decreased).

2) ROLE OF OROGRAPHY

The monsoon trough axis, extending from the heat low in Pakistan to the northern BoB, provides the background for LPS genesis and propagation (Sikka 1977; Goswami 1987; Krishnamurthy and Ajayamohan 2010). With an increase in

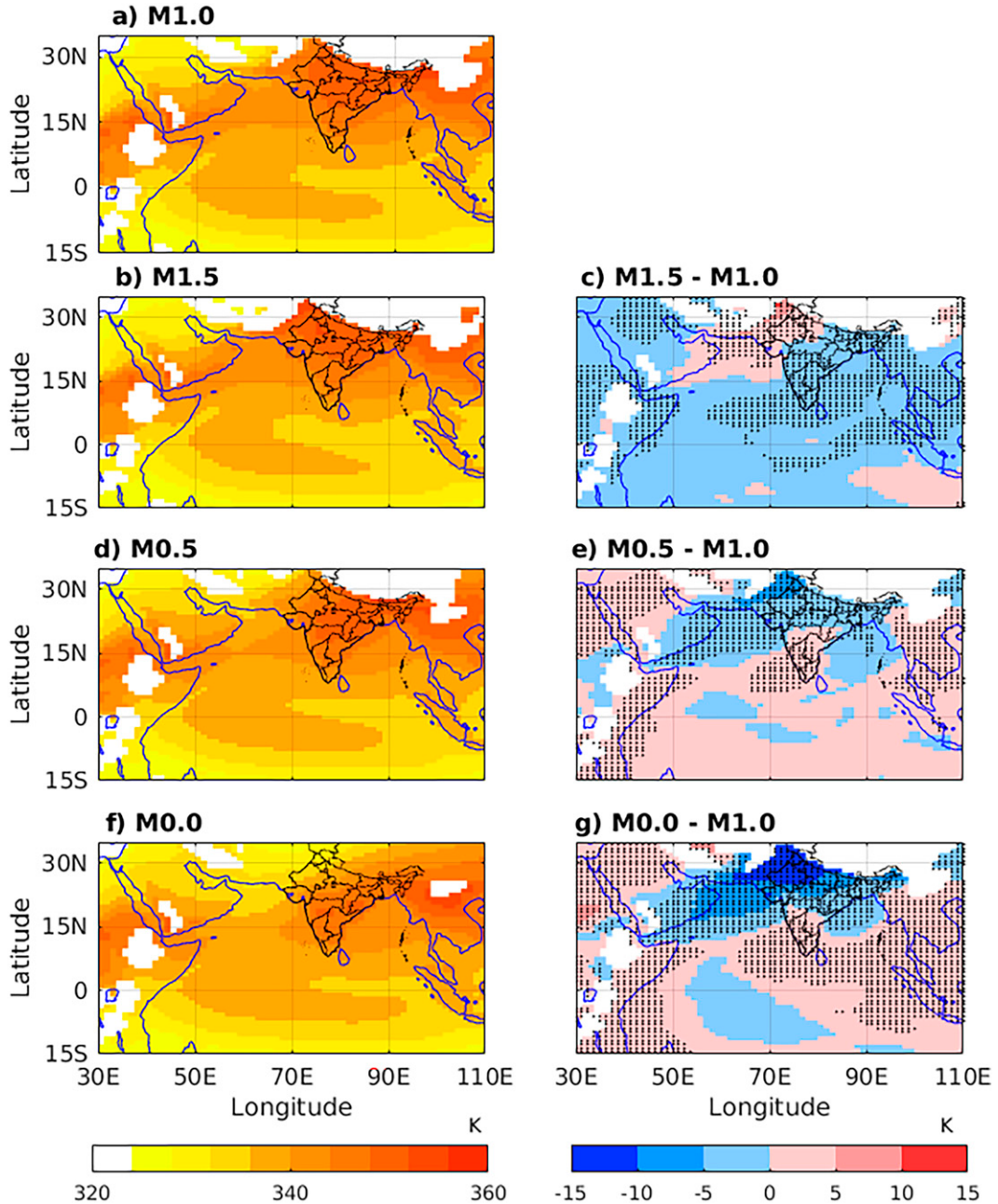


FIG. 6. The mean equivalent potential temperature at 875 hPa during the summer monsoon season (June–September) in the CESM simulations (a) M1.0, (b) M1.5, (d) M0.5, and (f) M0.0 over 37-yr periods, and anomalies in the (c) M1.5, (e) M0.5, and (g) M0.0 simulations relative to the M1.0 simulation. The white areas indicate the regions where the 875-hPa pressure level is below the orography. The hatching in the right panels shows regions where changes in the mean equivalent potential temperature are significant at a 95% confidence level as per the two-sample *t* test.

the height of THO, less intrusion of dry air and enhanced orographic precipitation occur as the trough axis moves northward toward the foothills of the Himalayas (Fig. 4) in the M1.5 simulation. There is a reduction in the simulated number of LPS of all categories and their collective duration in M1.5 compared to M1.0 (Table 2). A marginal reduction in the latitudinal extent of the genesis and track density of LPS

also occurs in M1.5 compared to M1.0, as the spread of the tracks around the median track is narrower in M1.5 (Fig. 8, Fig. S6). The synoptic activity index (SAI), which is an integrated metric that characterizes the activity of LPS at a location in terms of both the intensity (maximum wind speed) and number of systems (Ajayamohan et al. 2010), also shows a decrease in its spatial extent in the latitudinal direction (Fig. 9).

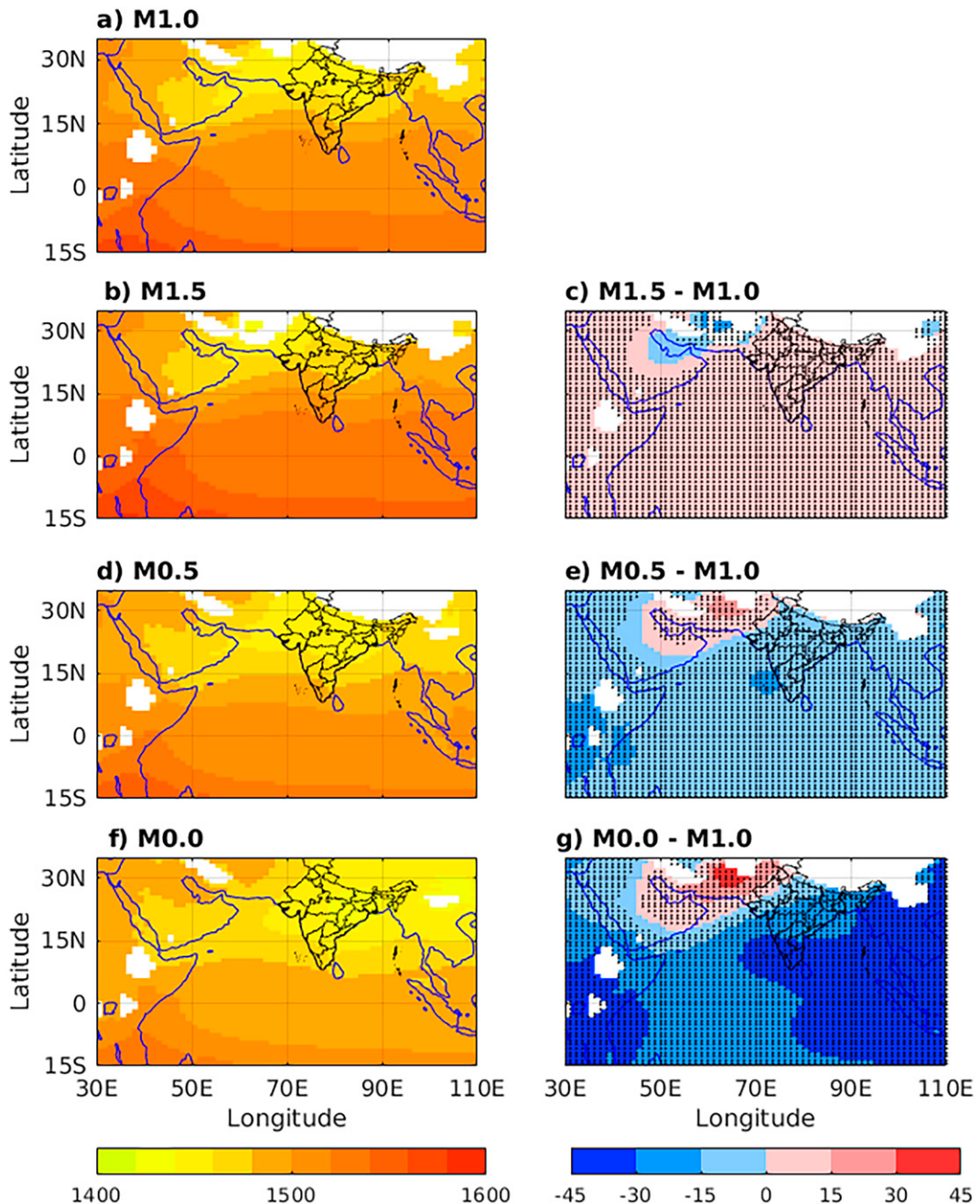


FIG. 7. The mean geopotential height ($\text{m}^2 \text{s}^{-2}$) at 850 hPa during the summer monsoon season (June–September) in the CESM simulations (a) M1.0, (b) M1.5, (d) M0.5, and (f) M0.0 over 37-yr periods, and anomalies in the (c) M1.5, (e) M0.5, and (g) M0.0 simulations relative to the M1.0 simulation. The white areas indicate the regions where the 850-hPa pressure level is below the orography. The hatching in the right panels shows regions where changes in the mean geopotential height are significant at a 95% confidence level as per the two-sample t test.

As a measure of orographic blocking, we calculate the vortex Froude number (VFN; Lin et al. 2005) as $V_{\max}/(Nh)$, where V_{\max} represents the maximum tangential velocity of the system, and N and h are the Brunt–Väisälä frequency and mountain height, respectively. The VFN can be interpreted as the ratio of the kinetic energy of the system to the potential energy required

to surmount the barrier. The lower the value of VFN, the higher is the orographic blocking by the mountain. When the VFN is less than 1.5, one study found the tracks of tropical systems to be discontinuous (Lin et al. 2005), although in a nonrotating frame at the laboratory scale, the limiting value of VFN for orographic blocking is much smaller (0.5; Baines 1987). The

TABLE 2. The annual mean number of different LPS categories (i.e., lows, depressions, deep depressions) and LPS days in the CESM simulations M1.0, M1.5, M0.5, and M0.0 estimated over 37-yr periods. The uncertainty is represented by one standard error.

CESM simulation	LPS	Lows	Depressions	Deep depressions	Depressions + deep depressions	LPS days
M1.5	12.4 ± 2.8	7.3 ± 2.4	4.4 ± 2.2	0.7 ± 0.8	5.1 ± 2.3	54.0 ± 12.4
M1.0	13.6 ± 2.6	8.0 ± 3.0	4.6 ± 1.8	1.0 ± 0.8	5.6 ± 1.9	63.1 ± 8.9
M0.5	16.1 ± 3.3	9.6 ± 3.5	5.5 ± 1.9	1.0 ± 0.9	6.5 ± 2.0	71.3 ± 10.3
M0.0	17.2 ± 3.0	10.2 ± 3.0	5.5 ± 1.9	1.5 ± 1.1	7.0 ± 1.9	81.1 ± 12.1

largest velocity for categorizing a system as a low is 8.5 m s^{-1} (IMD 2021), and the average height (between $80^{\circ}\text{--}100^{\circ}\text{E}$ and $30^{\circ}\text{--}40^{\circ}\text{N}$) of the THO in M1.5 is 5530 m. Taking a value of 0.01 s^{-1} for N (Lin et al. 2005), the VFN for M1.5 is estimated as 0.15, which is very small. Not surprisingly, this indicates that the THO can strongly block LPS that form near the foothills of the Himalayas. VFN values for M1.0 and M0.5 are 0.225 and 0.45, respectively.

Since the monsoon trough axis has moved northward in M1.5, most LPS form over land along the monsoon trough axis near the foothills of the Himalayas. Such systems are probably short lived as they propagate and reach the Himalayas faster, where they are subjected to strong orographic blocking. Therefore, these systems would decay before being identified by ATAGC as LPS because systems with a lifetime of fewer than two days are not categorized as LPS by our algorithm (ATAGC). Thus, we find that the northern extent of genesis and track density is reduced (Figs. 8 and 9). However, the zonal flow in M1.5 could occasionally split into upper (north) and lower (south) branches followed by a weakening of the upper branch resulting in trough formation near northern BoB (Fig. S7). Thus the position of the median track is nearly unchanged in the M1.5 simulation relative to M1.0.

When the height of THO is reduced to half in M0.5, there is an increase in the simulated number of LPS (Table 2) and the meridional extent of the LPS track density (in terms of the area occupied by the 66% of the tracks that lie closest to the median track) over the Indian subcontinent (Fig. 8). With a reduction in the height of THO the intrusion of dry extratropical air into the monsoon region increases (Fig. 6). This leads to a weaker MTG (Table 1), a southward shift of the trough axis (Fig. 4), and an extensive low pressure area as indicated by the spatial pattern of geopotential height (Fig. 7) over the Indian subcontinent. This, in turn, is associated with an increase and meridional spread in LPS genesis and track densities and expansion of the genesis area (Fig. 8). Similarly, when THO is completely removed in M0.0, the trough area further expands into the Tibetan and Himalayan areas (Fig. 7f) consistent with the formation and propagation of LPS not only over India but also in the neighboring areas to the north and northeast (Fig. 8, Fig. S8). Some LPS that form over the BoB and propagate northwestwards curve near northwest India and move into the Tibetan and Himalayan areas (Fig. S8). This is likely due to an interaction between the monsoon circulation and the subtropical jet stream (upper level westerlies) which have moved equatorward by about 4° in M0.0 compared to M1.0 (Fig. 10). Consequently, a spatially expanded track density over the Indian subcontinent is simulated (Fig. 8). Tracks that curve toward

the northeast (Fig. S8) have been also observed in the observational record during 1888–2003 (Fig. 1a of Krishnamurthy and Ajayamohan 2010). Figure 10 also shows the weakening and southeastward shift of the upper-level anticyclone when the height of THO is reduced, consistent with the reduction and southeastward shift in the maximum values of upper tropospheric temperature (Fig. 5). As shown by Ma et al. (2014), reductions in the height of orography like the THO allow the intrusion of dry extratropical air (Fig. 6), causing a reduction and southeastward shift in the location of maximum values of near-surface equivalent potential temperature and inhibition of convection by drying of the free-troposphere. Since the upper-tropospheric monsoon temperature maximum is maintained by convective coupling with near-surface air, this leads to a reduction in the magnitude and a southeastward shift in the location of maximum upper tropospheric temperature and the upper-level anticyclone. Abe et al. (2003) also simulated an increase in mean sea level pressure over THO on increasing the height of world orography as in our experiments. They attributed the increased sea level pressure to reduced surface temperature due to an increase in precipitation leading to an increase in ground wetness and a decrease in downwelling shortwave radiation at the surface due to an increase in cloudiness.

3) BAROTROPIC SHEAR AND THE GENESIS OF LPS

Monsoon LPS have been recently shown to draw energy for their growth from the meridional shear present in the basic state zonal wind, in a process similar to barotropic instability (Diaz and Boos 2019a,b). The mean monsoon circulation over north BoB ($80^{\circ}\text{--}90^{\circ}\text{E}$) is found to satisfy a necessary condition for barotropic instability (Fig. 11) in all four simulations, namely, a change in sign of the meridional gradient of the absolute vorticity. We calculate the mean meridional gradient (between 10° and 26°N) of 850-hPa zonal winds averaged over the longitudinal range $70^{\circ}\text{--}90^{\circ}\text{E}$ ($\partial U / \partial y$; obtained from Fig. 12a) as a measure for the degree to which the large-scale monsoon circulation might support barotropic growth. Estimates of this mean barotropic shear are -0.63 , -0.67 , -0.71 , and -0.81 s^{-1} in the M1.5, M1.0, M0.5, and M0.0 simulations, respectively (Table 1). Thus, with the decrease in the height of THO, the absolute magnitude of mean meridional shear of zonal wind is found to increase, implying that the conditions that might support barotropic growth increase in the core monsoon region. It is not just the absolute magnitude of meridional cyclonic shear that increases as the height of the THO is reduced, but also the latitudinal extent over which this shear exists (Fig. 12b).

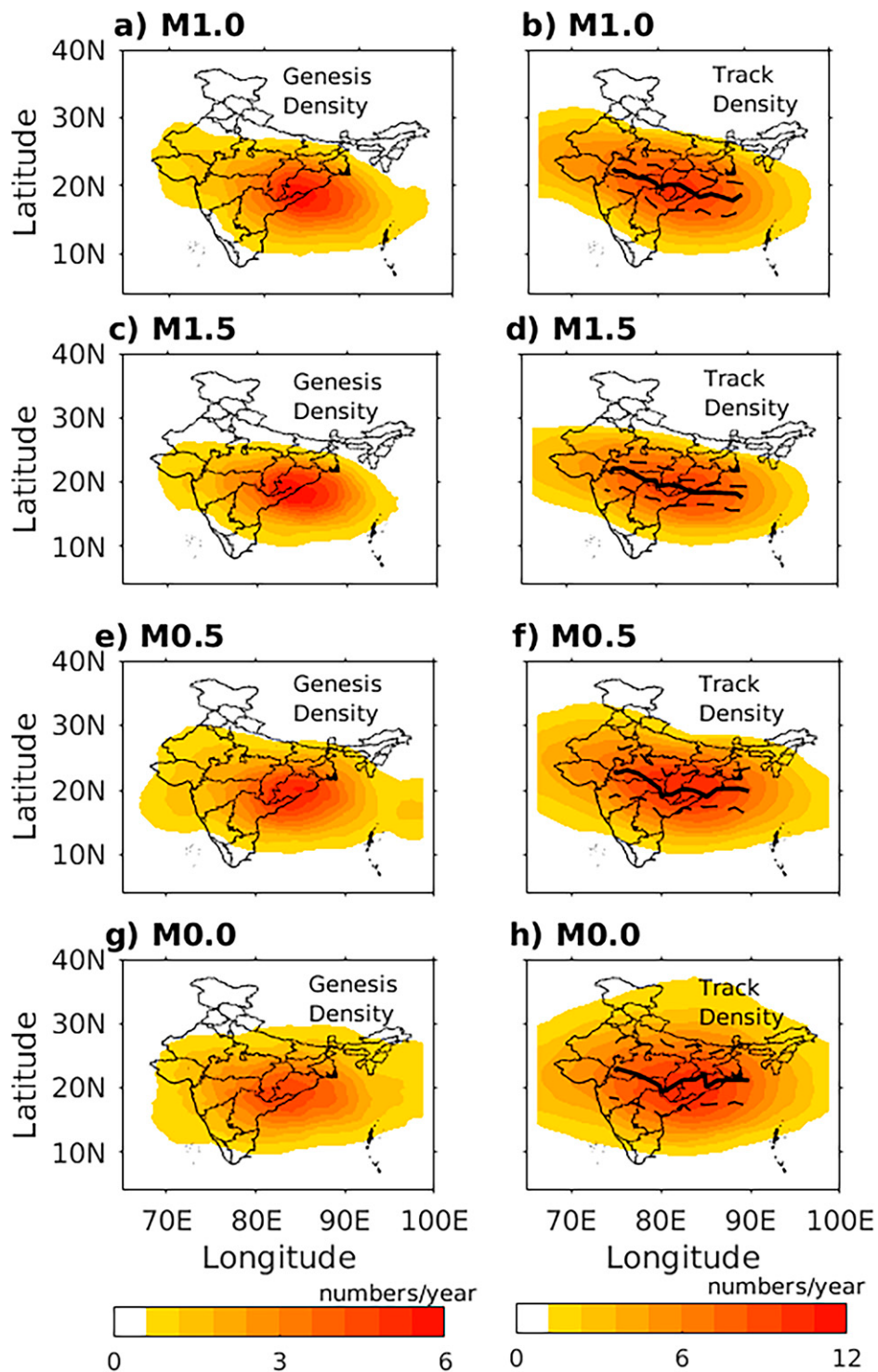


FIG. 8. (left) LPS genesis density (i.e., number of genesis locations per year within a 500-km radius of a location), and (right) LPS track density (i.e., number of tracks per year within a 500-km radius of a location) in the CESM simulations M1.0, M1.5, M0.5, and M0.0 over 37-yr periods. In each right panel, the solid black line indicates the median track, whereas the black dashed lines enclose 66% of the tracks around the median track. To construct the median track, the longitudinal belt extending from 76° to 90°E is divided into longitudinal sections of width 1° each, and the medians of latitudinal locations of tracks identified in the longitudinal sections are joined (Thomas et al. 2021).

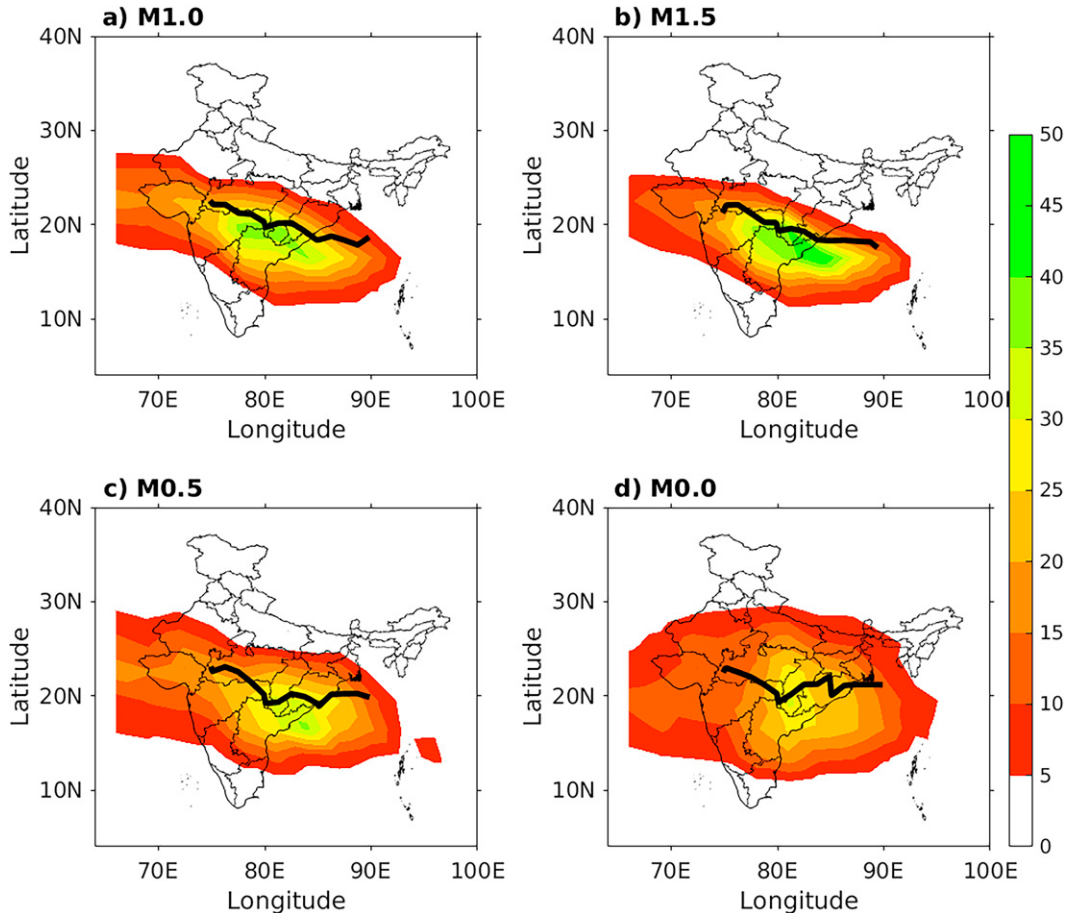


FIG. 9. Synoptic activity index (SAI) computed at $3^\circ \times 3^\circ$ resolution in the (a) M1.0, (b) M1.5, (c) M0.5, and (d) M0.0 simulations over 37-yr periods. In each panel, the thick black line denotes the median track of LPS.

The maximum of average zonal wind is found at 12.7°N in the M1.5 simulation, while the minimum exists at 25.9°N , giving a meridional extent of the cyclonic shear zone of 13.2° . The span increases to 16.0° in the M1.0 simulation and 17.0° in the M0.5 simulation. When the THO is completely removed, the extent of the shear zone increases to 18.9° (5.7° more than M1.5), spanning 8.9° – 27.8°N . With the reduction in the height of orography, the dry air intrusion (indicated by smaller values of equivalent potential temperature over India in Fig. 6) is enhanced, and the monsoon precipitation weakens (Fig. 3). The land becomes drier, and the surface temperature increases as cloudiness and precipitation decrease (Fig. S9, Figs. 13 and 14). The average surface temperature over India is 300.4, 301.6, 302.4, and 305.1 K in the M1.5, M1.0, M0.5, and M0.0 experiments, respectively. The low-level cyclonic circulation around India's monsoon trough also increases, as indicated by an increase in the curvature of the geopotential height at 850 hPa (Table 1). Thus, we find an intensification of the geostrophically balanced shallow heat low circulation over India when the height of THO is reduced. This is consistent with an increase in absolute vorticity over India with a decrease in height of THO (1.21 , 1.3 , 1.4 , and 1.5 s^{-1} for the M1.5, M1.0, M0.5, and M0.0 experiments, respectively). A lower-tropospheric,

shallow heat low is superimposed on the deep-tropospheric precipitating circulation in all of Earth's regional monsoons (Nie et al. 2010), and the shallow heat low circulation has been shown to strengthen as precipitation weakens in interannual variability in some regions (e.g., Shekhar and Boos 2017). Thus, with the reduction in the height of THO, an increase is found in the absolute magnitude and the latitudinal extent of the cyclonic shear of zonal wind around the South Asian heat low (Fig. 12), leading to stronger barotropic growth over a broader domain that we suggest increases the LPS activity area over the region (Fig. 8).

A southward latitudinal shift of the cyclonic shear zone is found in the spatial plot of meridional shear of zonal wind in M0.0 compared to the M1.0 simulation (Fig. S10). The shear conditions that favor the formation of LPS decrease at the location of maximum genesis density (corresponding to M1.0) when the height of THO is reduced. This causes a decrease in the maximum genesis density in M0.0 and M0.5 compared to M1.0 (Fig. 8). Thus, the maximum LPS genesis is reduced when the height of THO is decreased, but the density is spread over a wider domain (Fig. 8).

Although the number of stronger storms (i.e., depressions and deep depressions) increases as the orography is flattened, the number of lows also increases so that the fraction of LPS

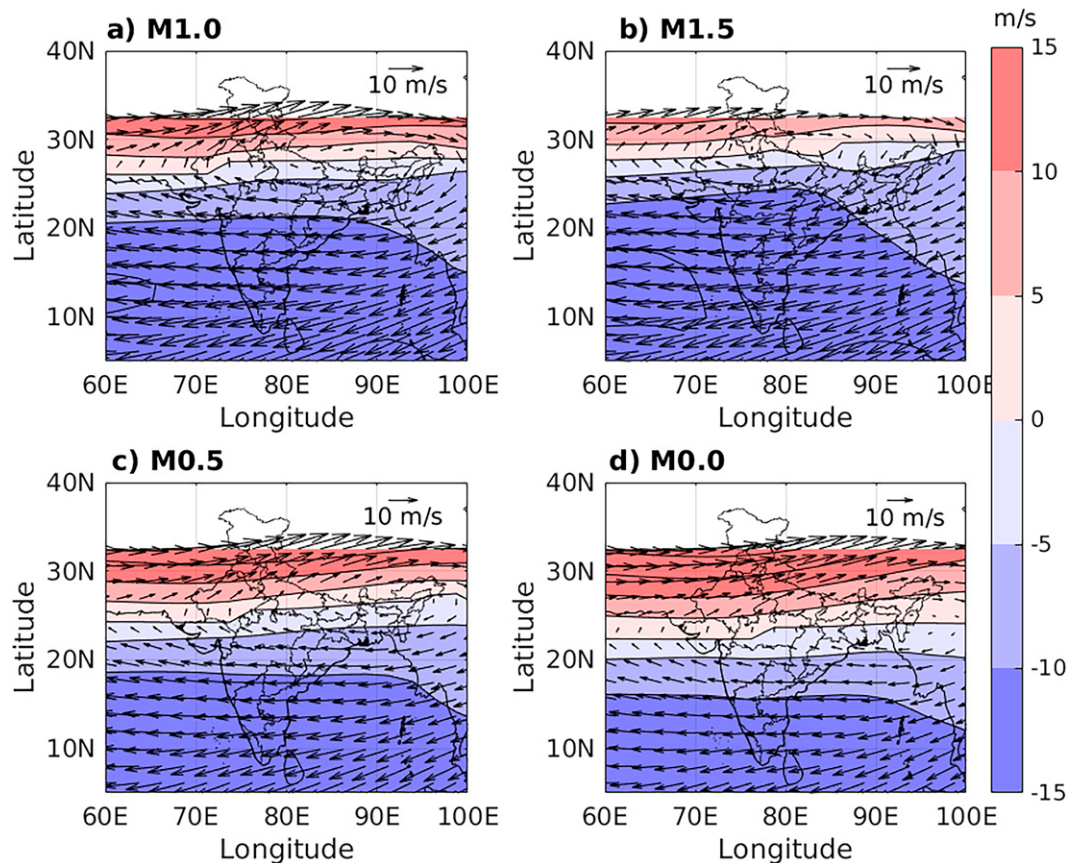


FIG. 10. The mean 200-hPa winds (m s^{-1}) during the summer monsoon season (June–September) over the Indian subcontinent in the CESM simulations (a) M1.0, (b) M1.5, (c) M0.5, and (d) M0.0. The subtropical jet moves equatorward by about 4° in M0.0 (around 24°) compared to M1.0 (around 28°) when THO is removed. The upper-level anti-cyclone moves southeastward. The shading represents the zonal wind velocity with positive values corresponding to westerlies and negative values to easterlies.

that are classified as depressions and deep depressions is nearly unchanged (Table 2). It is possible that this insensitivity of the intensity of the LPS distribution to THO height results from compensating changes in multiple factors. For example, a poleward moisture gradient has been argued to contribute to LPS intensification by enhancing moist convection on the western side of LPS (Adames and Ming 2018; Diaz and Boos 2021); the reduction in mean water vapor content and its northward gradient as THO height is reduced (Fig. S11) might thus reduce the intensification of lows into depressions, countering the positive influence of enhanced meridional shear on intensification. This reasoning is speculative, but we treat the question of the influence of THO height on the intensity distribution of LPS as a higher-order question that will be left for future work. A Fourier-based scale separation technique (Mishra 2018, 2021) could be used to enhance the current state of knowledge on various processes involved in LPS formation and propagation.

c. Precipitation associated with LPS

Monsoon LPS are the major rain bearers of much of continental South Asia (Yoon and Chen 2005; Hunt and Fletcher 2019;

Thomas et al. 2021). When precipitation within 1000 km of a LPS track (called LPS-related precipitation) is calculated over the Indian landmass, a decrease or increase in the height of THO by half its original value caused only a small change in this quantity. The spatial patterns of the average precipitation for different radial distances (in the range 500–1000 km) from the LPS center are similar, as shown in our recent study (Thomas et al. 2021). Therefore, without loss of generality, we have chosen the 1000 km radius to calculate the LPS-related precipitation. In the M1.0 simulation, the mean LPS-related precipitation is $10.70 \pm 1.0 \text{ mm day}^{-1}$ (Fig. S12, Table 1). The corresponding values in the M1.5 and M0.5 simulations are 10.56 ± 1.4 and $10.35 \pm 1.4 \text{ mm day}^{-1}$, respectively (Table 1). Here the uncertainty estimates are one standard deviation in mean precipitation within 1000 km of LPS track. Strong spatial correlation (r) is evident between LPS-related precipitation in (i) M1.5 and M1.0 ($r = 0.99$), and (ii) M0.5 and M1.0 ($r = 0.98$) (Fig. S12). However, when the THO is completely removed in the M0.0 simulation, a larger reduction (to $7.67 \pm 1.1 \text{ mm day}^{-1}$) is found in the mean LPS-related precipitation (Table 1). Even with an increase in the number of LPS, the decrease in the

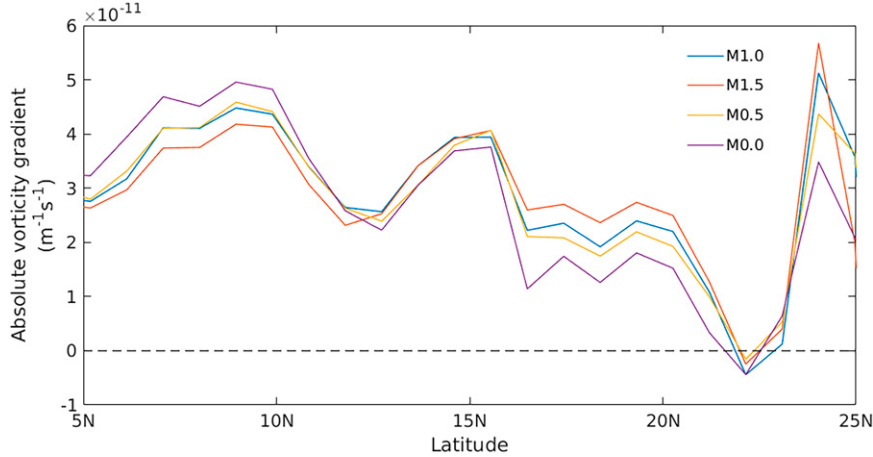


FIG. 11. Meridional gradient of absolute vorticity at 850 hPa ($\partial q_0 / \partial y = \beta - \partial^2 U / \partial y^2$) averaged over the longitudinal belt ($80^\circ\text{--}90^\circ\text{E}$) in the M1.0, M1.5, M0.5, and M0.0 simulations over 37-yr periods. Barotropic instability occurs when the absolute vorticity gradient changes its sign (Pedlosky 1979). A sign change of the absolute vorticity gradient occurs around 22°N in all the simulations.

amount of precipitable water (Table 1, Fig. S11) is the likely cause for a decrease in the magnitude of LPS-related precipitation in M0.0. This indicates that THO enhances monsoon and LPS-related precipitation by acting as a barrier to dry extratropical air (Boos and Kuang 2010).

According to a recent study (Hunt and Fletcher 2019), around 44% of monsoon precipitation over India is LPS-related in the observational dataset. Our simulated value in M1.0 of 37% is close to this value (Table 1). The percentage of LPS-related monsoon precipitation decreases to 31% in the M1.5 simulation owing to a decrease in the number of LPS with an increase in the height of THO. However, as the number of LPS

increases with the decrease in the height of orography, percentage contribution by LPS to total monsoon precipitation increases to 44% and 57% in the M0.5 and M0.0 simulations, respectively (Table 1).

In CESM, the mean summer monsoon precipitation over the Indian landmass on LPS days is $9.16 \pm 0.7 \text{ mm day}^{-1}$ in the M1.0 simulation (Table 1). Similar to the behavior of mean summer monsoon precipitation over India, with the reduction in the height of THO, there is a reduction in simulated precipitation over India on LPS days in the case of M0.5 ($8.14 \pm 1.0 \text{ mm day}^{-1}$) and M0.0 ($5.22 \pm 0.9 \text{ mm day}^{-1}$), respectively (Table 1). In comparison, an increase in the height of

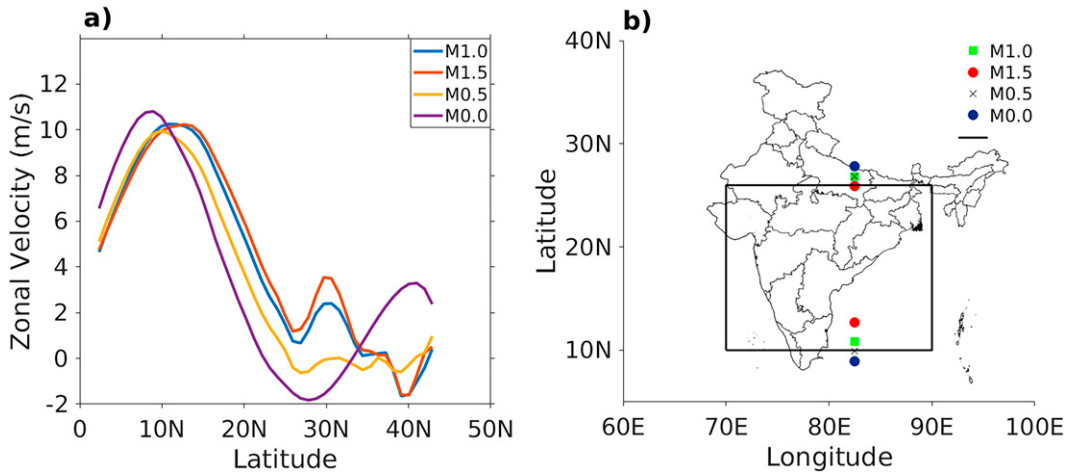


FIG. 12. (a) The mean 850-hPa zonal winds averaged over the longitudinal belt ($70^\circ\text{--}90^\circ\text{E}$) in the M1.0, M1.5, M0.5, and M0.0 simulations over 37-yr periods. Meridional shear of zonal wind (which is an indicator for barotropic instability) is determined for each simulation as the slope of the mean zonal wind between 10° and 26°N . (b) The black outlined box indicates the domain used for calculation of meridional shear in (a), and colored dots indicate the latitudinal extent of cyclonic barotropic shear estimated as the latitudinal distance between the maximum and minimum zonal winds in (a) for each experiment between 2° and 30°N .

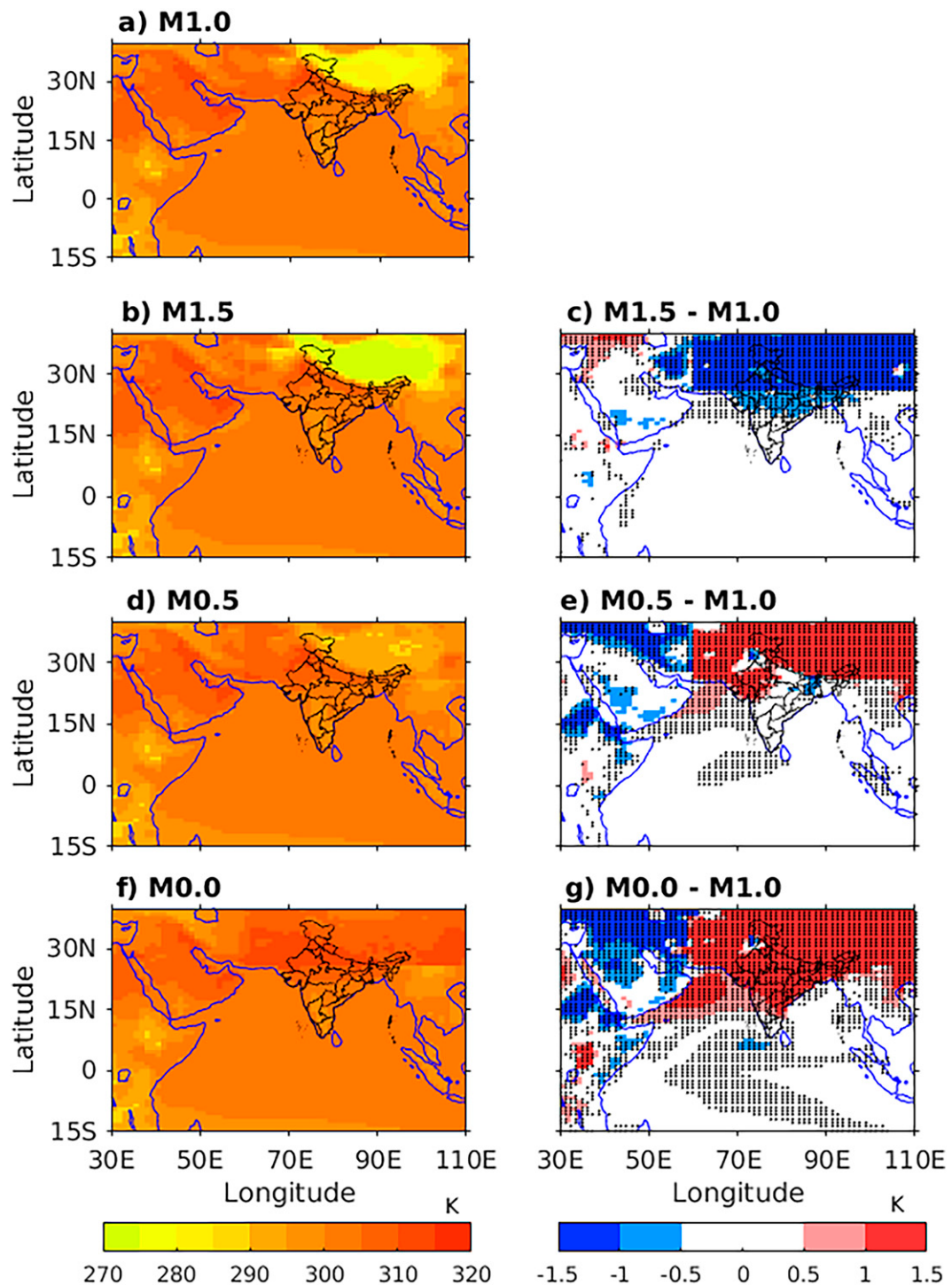


FIG. 13. Mean surface temperature during the summer monsoon season (June–September) in the CESM simulations (a) M1.0, (b) M1.5, (d) M0.5, and (f) M0.0 over 37-yr periods, and anomalies in the (c) M1.5, (e) M0.5, and (g) M0.0 simulations relative to the M1.0 simulation. The hatching in the right panels shows regions where changes in the mean surface temperature are significant at a 95% confidence level as per the two-sample *t* test.

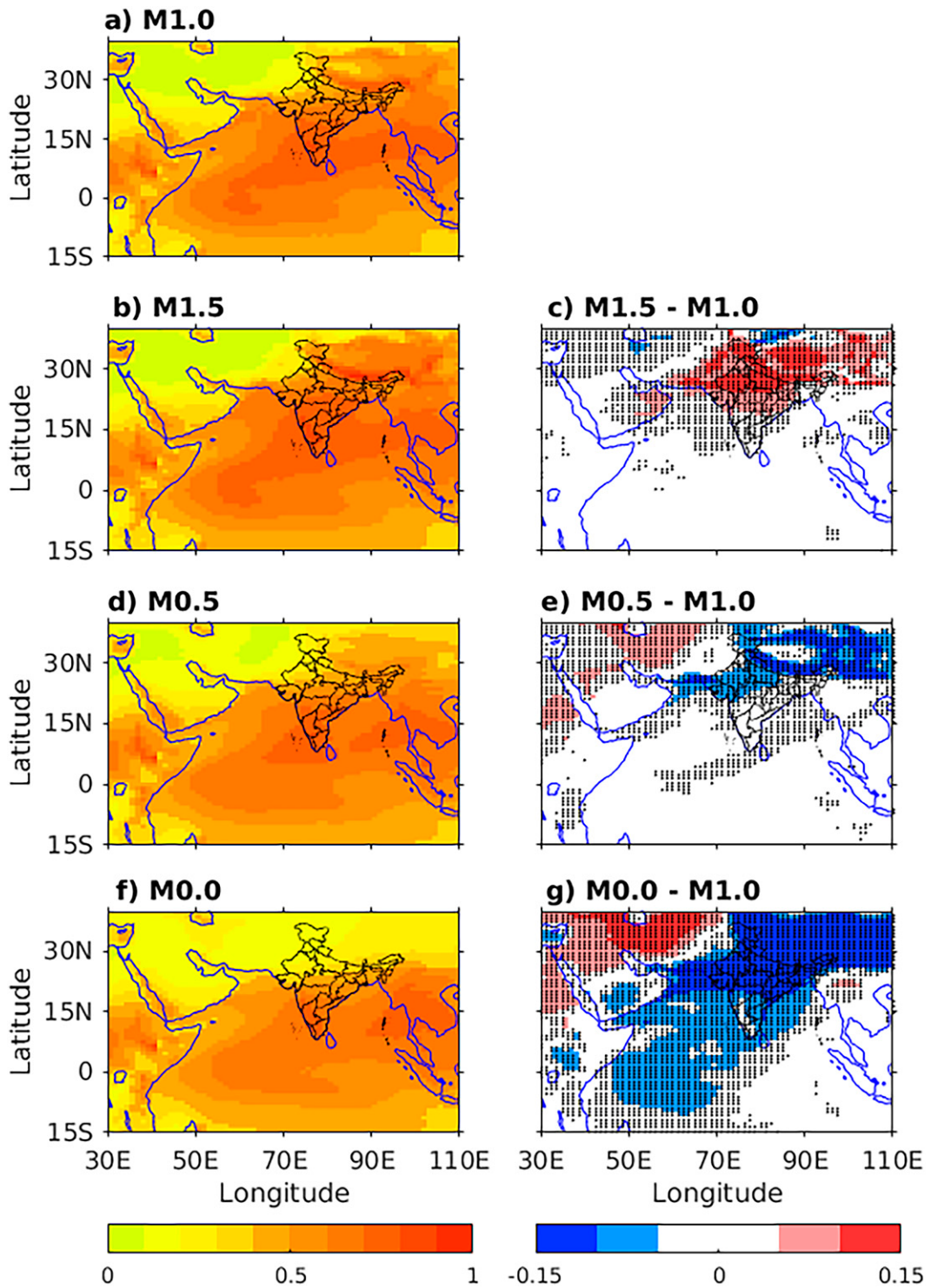


FIG. 14. Mean vertically integrated total cloud (fraction) during the summer monsoon season (June–September) in the CESM simulations (a) M1.0, (b) M1.5, (d) M0.5, and (f) M0.0 over 37-yr periods, and anomalies in the (c) M1.5, (e) M0.5, and (g) M0.0 simulations relative to the M1.0 simulation. The hatching in the right panels shows regions where changes in the mean vertically integrated total cloud are significant at a 95% confidence level as per the two-sample *t* test.

THO in M1.5 leads to an increase in precipitation over India on LPS days ($9.81 \pm 0.9 \text{ mm day}^{-1}$; [Table 1](#)). The major difference in simulated precipitation (with respect to that in M1.0) is noted along the foothills of the Himalayas in all three experiments, namely, M1.5, M0.5, and M0.0 ([Fig. S13](#)). Overall, our simulations indicate that orographic rainfall plays a major role in increasing/decreasing the precipitation over the country on LPS days. A large decrease in LPS-related precipitation is simulated along the core monsoon region of central India only in the M0.0 simulation ([Fig. S12](#)), indicating that the presence or absence of THO has a major influence on LPS-related precipitation in the core monsoon region.

Monsoon LPS are the major contributor to extreme precipitation events occurring during the summer monsoon in India ([Thomas et al. 2021](#)). A precipitation event is called extreme if the daily precipitation is greater than 64.5 mm day^{-1} ([IMD 2021](#)). About 48% of extreme precipitation events during monsoon season are LPS-related in the M1.0 simulation. The percentage decreases to 38.5% in the M1.5 simulation ([Table 1](#)), even though there is an increase in the number of extreme events (by 10.1%; not shown in table) compared to the M1.0 simulation. This can be attributed to a decrease in the number of LPS in M1.5 compared to M1.0. In contrast, in the M0.5 and M0.0 simulations, there is a decrease in the number of monsoon extreme events (by 43.5% and 66.9%, respectively) compared to M1.0, together with an overall decrease in summer monsoon precipitation. However, a larger percentage of the extremes (62.7% in M0.5 and 85.8% in M0.0) are found to be LPS-related ([Table 1](#)), which could be attributed to a significant increase in the number of LPS. Similarly, of the total amount of monsoon precipitation occurring as extreme precipitation over India, 47.3% is LPS-related in the M1.0 simulation, 38.7%, 63.1%, and 87.0% in the M1.5, M0.5, and M0.0 simulations, respectively ([Table 1](#)).

4. Summary and conclusions

In this study, we have investigated the influence of THO on monsoon LPS using a fully coupled version of climate model CESM1.2.2. Four experiments are performed in which the height of THO is changed to 1.5, 1.0, 0.5, and 0.0 times its original value. Even though there is a decrease in simulated mean summer monsoon precipitation and circulation with a reduction in the height of THO, the frequency and latitudinal extent of LPS increase. A schematic of key changes in the upper, middle, and lower levels when the height of THO is decreased is shown in [Fig. 15](#). A southward shift and an increase in the meridional extent of the low level cyclonic meridional shear ([Fig. 15](#)) are simulated when the height of THO is decreased. The dry extratropical air intrusion due to the reduction in the height causes the maxima of upper tropospheric temperature ([Fig. 5](#)) and the associated low-level equivalent potential temperature (through quasi equilibrium; [Fig. 6](#)) to decrease and shift southeastwards ([Fig. 15](#)). The decrease in monsoon precipitation and the associated increase in surface temperature ([Fig. 13](#)) leads to an intensification of the trough ([Fig. 7](#)), geographically associated westerlies ([Fig. 12](#)), and the meridional shear. Recent literature shows that LPS draw their energy from barotropic growth

coupled with precipitating convection ([Diaz and Boos 2019a,b](#)). When the height of THO is reduced or even removed, an increase in the mean meridional cyclonic shear and its latitudinal extent is simulated during the monsoon season ([Fig. 15](#)) which leads to an increase in the number of LPS and the latitudinal extent of their formation and propagation.

The LPS-related precipitation (i.e., which occurs within 1000 km of LPS tracks) remains almost unchanged when the height of THO is increased or decreased by half its original height. The changes in precipitation for those cases are about 1.3% and 3.3%, respectively. In contrast, precipitation on LPS days shows a significant change, indicating that the orographic rainfall (near the foothills of the Himalayas) plays a major role in increasing or decreasing the rain associated with LPS. Further, a decrease in the total number of precipitation extremes and a 40% increase in the percentage of LPS-related precipitation extremes are simulated in the absence of THO.

Our results are consistent with earlier studies ([Ashfaq 2020](#); [Ashfaq et al. 2009](#)) which showed that models that simulate a stronger MTG tend to also simulate a northward shift in the monsoon trough ([Rastogi et al. 2018](#)); here we argue that the weakening and increased proximity of low-level meridional shear zone that accompanies that northward shift in the trough cause reduced LPS genesis. Among the 11 CMIP5 models analyzed by [Ashfaq et al. \(2009\)](#), the Hadley models and ACCESS1-0 had the strongest MTG and simulated weak LPS activity over the BoB ([Rastogi et al. 2018](#)). This is consistent with earlier studies that showed the mechanisms influencing the MTG strongly impact LPS formation and propagation.

There are some limitations to our study. First, we have performed only a single simulation for each experiment, and an ensemble of simulations would be desirable. However, each simulation is multiple decades long, and the consistency in the results among the experiments (the consistent decrease in the frequency of LPS when the height of THO is increased) lends confidence in our results. Second, the simulations presented are from a single climate model, and LPS tracks are identified using a single tracking algorithm. An analysis of an ensemble of simulations from multiple climate models and applying multiple tracking algorithms ([Vishnu et al. 2020](#)) on those to infer changes in LPS characteristics (genesis area, track density) and LPS-related precipitation (including extremes) would help to test the robustness of the conclusions drawn in this article. Analysis using models with higher vertical resolution would also aid in testing the robustness of the results obtained, although prior work has shown that South Asian LPS can be simulated with roughly 30 vertical levels in the atmosphere ([Adames and Ming 2018](#)).

Finally, because of the coarse resolution of our climate model simulations, the orography may also be highly smoothed compared to observed orography. Despite these limitations, our study confirms the reduction in summer monsoon precipitation and monsoon circulation on the removal of THO. That aspect of this paper merely confirms prior work showing how orography alters mean monsoon strength (e.g., [Hahn and Manabe 1975](#); [Chakraborty et al. 2006](#); [Boos and Kuang 2010](#)), but it does so in the context needed to understand associated LPS changes. Furthermore, for the first time, we have investigated

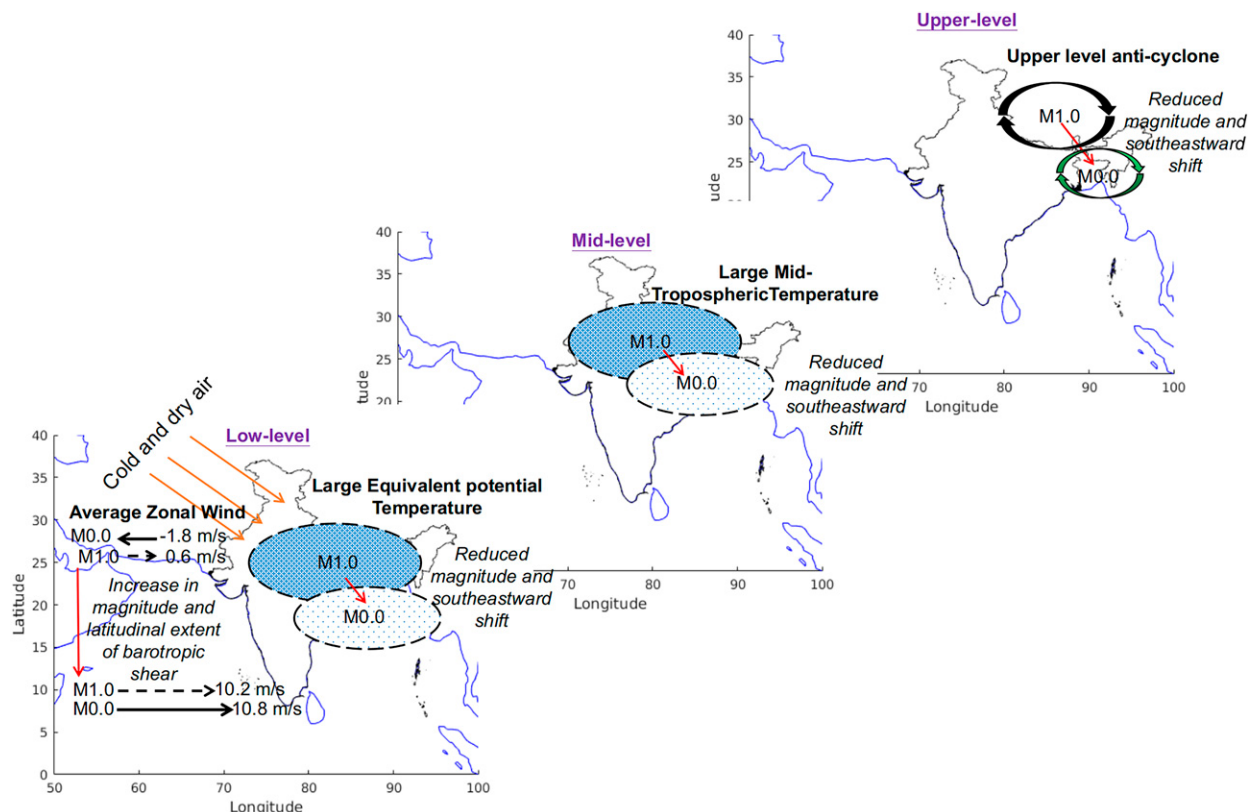


FIG. 15. Schematic diagram showing the mechanism associated with a decrease in the height of Tibet and Himalayan orography (THO) on LPS activity over India. With a decrease in the height of THO, the dry air intrusion into the Indian mainland increases, which leads to a reduction in the magnitude and southeastward shift of maximum low-level equivalent potential temperature. The quasi-convective equilibrium associated with the monsoon system leads to a reduction in the magnitude and southeastward shift of maximum midtropospheric temperature and upper-level anticyclone. The dilution of moist energy causes a decrease in the monsoon circulation and an equatorward shift of the location of the monsoon trough. The northerlies displace the westerlies over the northern part of India, leading to an increase in the magnitude and latitudinal extent of barotropic cyclonic shear. This, in turn, causes an increase in the number and latitudinal extent of genesis area of LPS over the country.

the role of THO on LPS activity in India and showed that the number and latitudinal extent of LPS activity would increase on the removal of THO. This anticorrelation between mean monsoon strength and the LPS number/spatial extent of LPS activity is an unexpected and important finding, meriting further investigation to see if it might also hold for other forcings.

Acknowledgments. We acknowledge the Supercomputer Education and Research Centre, Indian Institute of Science, Bangalore, for providing the computational facility required for running the CESM model. The first author acknowledges the Ministry of Human Resource Development, Government of India, for the Prime Minister's Research Fellowship. The second and third authors acknowledge the support from the Ministry of Earth Sciences through the Project MoES/PAMC/H&C/41/2013-PC-II. The authors also acknowledge the support of Department of Science and Technology (DST) through the grant DST/CCP/NMSKCC/210/2022(C).

Data availability statement. Organizations whose data were used in the present study include European Center for Medium

Range Forecasts (ECMWF) (data available at <https://apps.ecmwf.int/datasets/data/interim-full-daily/levtype=sfc/>) and India Meteorological Department (IMD) (data available at https://www.imdpune.gov.in/Clim_Pred_LRF_New/Grided_Data_Download.html). Details of tracking algorithm used can be obtained from Thomas et al. (2021). The model used in this study CESM1.2.2 can be downloaded using svn (details provided at: http://www.cesm.ucar.edu/models/cesm1.2/tags/index.html#CESM1_2_2). LPS tracks simulated in this research are available at Zenodo repository (<https://doi.org/10.5281/zenodo.5728713>).

REFERENCES

- Abe, M., A. Kitoh, and T. Yasunari, 2003: An evolution of the Asian summer monsoon associated with mountain uplift—Simulation with the MRI atmosphere-ocean coupled GCM. *J. Meteor. Soc. Japan*, **81**, 909–933, <https://doi.org/10.2151/jmsj.81.909>.
- Adames, A. F., and Y. Ming, 2018: Moisture and moist static energy budgets of South Asian monsoon low pressure systems in GFDL AM4.0. *J. Atmos. Sci.*, **75**, 2107–2123, <https://doi.org/10.1175/JAS-D-17-0309.1>.

- Ajayamohan, R. S., 2007: Simulation of South-Asian summer monsoon in a GCM. *Pure Appl. Geophys.*, **164**, 2117–2140, <https://doi.org/10.1007/s00024-007-0249-9>.
- , W. J. Merryfield, and V. V. Kharin, 2010: Increasing trend of synoptic activity and its relationship with extreme rain events over Central India. *J. Climate*, **23**, 1004–1013, <https://doi.org/10.1175/2009JCLI2918.1>.
- Ashfaq, M., 2020: Topographic controls on the distribution of summer monsoon precipitation over South Asia. *Earth Syst. Environ.*, **4**, 667–683, <https://doi.org/10.1007/s41748-020-00196-0>.
- , Y. Shi, W. W. Tung, R. J. Trapp, X. J. Gao, J. S. Pal, and N. S. Diffenbaugh, 2009: Suppression of South Asian summer monsoon precipitation in the 21st century. *Geophys. Res. Lett.*, **36**, L01704, <https://doi.org/10.1029/2008GL036500>.
- Baines, P. G., 1987: Upstream blocking and airflow over mountains. *Annu. Rev. Fluid Mech.*, **19**, 75–95, <https://doi.org/10.1146/annurev.fl.19.010187.000451>.
- Bettinelli, P., J. P. Avouac, M. Flouzat, F. Jouanne, L. Bollinger, P. Willis, and G. Chitrakar, 2006: Plate motion of India and interseismic strain in the Nepal Himalaya from GPS and DORIS measurements. *J. Geod.*, **80**, 567–589, <https://doi.org/10.1007/s00190-006-0030-3>.
- Boos, W., and Z. Kuang, 2010: Dominant control of the South Asian monsoon by orographic insulation versus plateau heating. *Nature*, **463**, 218–222, <https://doi.org/10.1038/nature08707>.
- , and J. V. Hurley, 2013: Thermodynamic bias in the multi-model mean boreal summer monsoon. *J. Climate*, **26**, 2279–2287, <https://doi.org/10.1175/JCLI-D-12-00493.1>.
- , and Z. Kuang, 2013: Sensitivity of the South Asian monsoon to elevated and non-elevated heating. *Sci. Rep.*, **3**, 1192, <https://doi.org/10.1038/srep01192>.
- Chakraborty, A., R. S. Nanjundiah, and J. Srinivasan, 2002: Role of Asian and African orography in Indian summer monsoon. *Geophys. Res. Lett.*, **29**, 1989, <https://doi.org/10.1029/2002GL015522>.
- , —, and —, 2006: Theoretical aspects of the onset of Indian summer monsoon from perturbed orography simulations in a GCM. *Ann. Geophys.*, **24**, 2075–2089, <https://doi.org/10.5194/angeo-24-2075-2006>.
- Diaz, M., and W. R. Boos, 2019a: Barotropic growth of monsoon depressions. *Quart. J. Roy. Meteor. Soc.*, **145**, 824–844, <https://doi.org/10.1002/qj.3467>.
- , and —, 2019b: Monsoon depression amplification by moist barotropic instability in a vertically sheared environment. *Quart. J. Roy. Meteor. Soc.*, **145**, 2666–2684, <https://doi.org/10.1002/qj.3585>.
- , and —, 2021: The influence of surface heat fluxes on the growth of idealized monsoon depressions. *J. Atmos. Sci.*, **78**, 2013–2027, <https://doi.org/10.1175/JAS-D-20-0359.1>.
- Doney, S. C., K. Lindsay, I. Fung, and J. John, 2006: Natural variability in a stable, 1000-yr global coupled climate-carbon cycle simulation. *J. Climate*, **19**, 3033–3054, <https://doi.org/10.1175/JCLI3783.1>.
- Goswami, B. N., 1987: A mechanism for the west-north-west movement of monsoon depressions. *Nature*, **326**, 376–378, <https://doi.org/10.1038/326376a0>.
- , and P. K. Xavier, 2005: ENSO control on the South Asian monsoon through the length of the rainy season. *Geophys. Res. Lett.*, **32**, L18717, <https://doi.org/10.1029/2005GL023216>.
- Hahn, D., and S. Manabe, 1975: The role of mountains in the South Asian monsoon circulation. *J. Atmos. Sci.*, **32**, 1515–1541, [https://doi.org/10.1175/1520-0469\(1975\)032<1515:TROMIT>2.0.CO;2](https://doi.org/10.1175/1520-0469(1975)032<1515:TROMIT>2.0.CO;2).
- Hanf, F. S., and H. Annamalai, 2020: Systematic errors in South Asian monsoon precipitation: Process-based diagnostics and sensitivity to entrainment in NCAR models. *J. Climate*, **33**, 2817–2840, <https://doi.org/10.1175/JCLI-D-18-0495.1>.
- He, B., 2017: Influences of elevated heating effect by the Himalaya on the changes in Asian summer monsoon. *Theor. Appl. Climatol.*, **128**, 905–917, <https://doi.org/10.1007/s00704-016-1746-5>.
- Hunke, E. C., and W. H. Lipscomb, 2008: CICE: The Los Alamos Sea Ice Model, documentation and software, version 4.0. Los Alamos National Laboratory Tech. Rep. LACC-06-012, 76 pp.
- Hunt, K. M. R., and D. J. Parker, 2016: The movement of Indian monsoon depressions by interaction with image vortices near the Himalayan wall. *Quart. J. Roy. Meteor. Soc.*, **142**, 2224–2229, <https://doi.org/10.1002/qj.2812>.
- , and J. K. Fletcher, 2019: The relationship between Indian monsoon rainfall and low-pressure systems. *Climate Dyn.*, **53**, 1859–1871, <https://doi.org/10.1007/s00382-019-04744-x>.
- Hurley, J. V., and W. R. Boos, 2015: A global climatology of monsoon low-pressure systems. *Quart. J. Roy. Meteor. Soc.*, **141**, 1049–1064, <https://doi.org/10.1002/qj.2447>.
- Hurrell, J. W., and Coauthors, 2013: The Community Earth System Model: A framework for collaborative research. *Bull. Amer. Meteor. Soc.*, **94**, 1339–1360, <https://doi.org/10.1175/BAMS-D-12-00121.1>.
- IMD, 2021: Terminologies and glossary. India Meteorological Department, 19 pp., <https://img.indiaonline.in/weather/weather-glossary.pdf>.
- Joseph, P. V., and S. Sijikumar, 2004: Intraseasonal variability of the low-level jet stream of the Asian summer monsoon. *J. Climate*, **17**, 1449–1458, [https://doi.org/10.1175/1520-0442\(2004\)017<1449:IVOTLJ>2.0.CO;2](https://doi.org/10.1175/1520-0442(2004)017<1449:IVOTLJ>2.0.CO;2).
- Keshavamurti, R. N., V. Satyan, and B. N. Goswami, 1978: Indian summer monsoon cyclogenesis and its variability. *Nature*, **274**, 576–578, <https://doi.org/10.1038/274576a0>.
- Kitoh, A., 1997: Mountain uplift and surface temperature changes. *Geophys. Res. Lett.*, **24**, 185–188, <https://doi.org/10.1029/96GL03953>.
- Krishnamurthy, V., and R. S. Ajayamohan, 2010: Composite structure of monsoon low pressure systems and its relation to Indian rainfall. *J. Climate*, **23**, 4285–4305, <https://doi.org/10.1175/2010JCLI2953.1>.
- Lin, Y., S. Chen, C. Hill, and C. Huang, 2005: Control parameters for the influence of a mesoscale mountain range on cyclone track continuity and deflection. *J. Atmos. Sci.*, **62**, 1849–1866, <https://doi.org/10.1175/JAS3439.1>.
- Ma, D., W. Boos, and Z. Kuang, 2014: Effects of orography and surface heat fluxes on the South Asian summer monsoon. *J. Climate*, **27**, 6647–6659, <https://doi.org/10.1175/JCLI-D-14-00138.1>.
- Mishra, S. K., 2018: On the evolution of planetary-scale fields and genesis of monsoon depressions over the Indian region. *Quart. J. Roy. Meteor. Soc.*, **144**, 129–141, <https://doi.org/10.1002/qj.3189>.
- , 2021: Development of a monsoon depression and its interaction with the large-scale background: A case study. *Mon. Wea. Rev.*, **149**, 3627–3646, <https://doi.org/10.1175/MWR-D-21-0084.1>.
- Mooley, D. A., and J. Shukla, 1987: Characteristics of the westward-moving summer monsoon low pressure systems over the Indian region and their relationship with the monsoon rainfall. University of Maryland Center for Ocean-Land-Atmosphere Interactions Rep., 47 pp.
- Neale, R. B., J. Richter, S. Park, P. H. Lauritzen, S. J. Vavrus, P. J. Rasch, and M. Zhang, 2013: The mean climate of the Community Atmosphere Model (CAM4) in forced SST and

- fully coupled experiments. *J. Climate*, **26**, 5150–5168, <https://doi.org/10.1175/JCLI-D-12-00236.1>.
- Nie, J., W. R. Boos, and Z. Kuang, 2010: Observational evaluation of a convective quasi-equilibrium view of monsoons. *J. Climate*, **23**, 4416–4428, <https://doi.org/10.1175/2010JCLI3505.1>.
- Okajima, H., and S. P. Xie, 2007: Orographic effects on the northwestern Pacific monsoon: Role of air-sea interaction. *Geophys. Res. Lett.*, **34**, L21708, <https://doi.org/10.1029/2007GL032206>.
- Oleson, K. W., and Coauthors, 2010: Technical description of version 4.0 of the Community Land Model (CLM). NCAR Tech. Note NCAR/TN-478+STR, 257 pp., <https://doi.org/10.5065/D6FB50WZ>.
- Park, H., J. C. H. Chiang, and S. Bordoni, 2012: The mechanical impact of the Tibetan Plateau on the seasonal evolution of the South Asian monsoon. *J. Climate*, **25**, 2394–2407, <https://doi.org/10.1175/JCLI-D-11-00281.1>.
- Pedlosky, J., 1979: *Geophysical Fluid Dynamics*. 1st ed. Springer, 624 pp., <https://doi.org/10.1007/978-1-4684-0071-7>.
- Rastogi, D., M. Ashfaq, L. R. Leung, S. Ghosh, A. Saha, K. Hodges, and K. Evans, 2018: Characteristics of Bay of Bengal monsoon depressions in the 21st century. *Geophys. Res. Lett.*, **45**, 6637–6645, <https://doi.org/10.1029/2018GL078756>.
- Shekhar, R., and W. R. Boos, 2017: Weakening and shifting of the Saharan shallow meridional circulation during wet years of the West African monsoon. *J. Climate*, **30**, 7399–7422, <https://doi.org/10.1175/JCLI-D-16-0696.1>.
- Sikka, D. R., 1977: Some aspects of the life history, structure and movement of monsoon depressions. *Pure Appl. Geophys.*, **115**, 1501–1529, <https://doi.org/10.1007/BF00874421>.
- Smith, R. D., and Coauthors, 2010: The Parallel Ocean Program (POP) reference manual: Ocean component of the Community Climate System Model (CCSM) and Community Earth System Model (CESM). Los Alamos National Laboratory Tech. Rep. LAUR-10-01853, 141 pp.
- Thomas, T. M., G. Bala, and V. V. Srinivas, 2021: Characteristics of the monsoon low pressure systems in the Indian subcontinent and the associated extreme precipitation events. *Climate Dyn.*, **56**, 1859–1878, <https://doi.org/10.1007/s00382-020-05562-2>.
- , —, and S. V. Vemavarapu, 2022: CESM simulation of monsoon low pressure systems over India. *Int. J. Climatol.*, **42**, 5964–5984, <https://doi.org/10.1002/joc.7571>.
- Vishnu, S., W. R. Boos, P. A. Ullrich, and T. A. O'Brien, 2020: Assessing historical variability of South Asian monsoon lows and depressions with an optimized tracking algorithm. *J. Geophys. Res. Atmos.*, **125**, e2020JD032977, <https://doi.org/10.1029/2020JD032977>.
- Wu, C.-H., W.-R. Huang, and S.-Y. Wang, 2018: Role of Indo-china Peninsula topography in precipitation seasonality over East Asia. *Atmosphere*, **9**, 255, <https://doi.org/10.3390/atmos9070255>.
- Wu, G., Y. Liu, B. He, B. Bao, D. Anmin, and J. Fei-Fei, 2012: Thermal controls on the Asian summer monsoon. *Sci. Rep.*, **2**, 404, <https://doi.org/10.1038/srep00404>.
- Yao, Z., Y. Tang, D. Chen, L. Zhou, X. Li, T. Lian, and S. Ul Islam, 2016: Assessment of the simulation of Indian Ocean Dipole in the CESM—Impacts of atmospheric physics and model resolution. *J. Adv. Model. Earth Syst.*, **8**, 1932–1952, <https://doi.org/10.1002/2016MS000700>.
- Yoon, J. H., and T. C. Chen, 2005: Water vapor budget of the Indian monsoon depression. *Tellus*, **57A**, 770–782, <https://doi.org/10.3402/tellusa.v57i5.14737>.
- Zhang, R., D. Jiang, Z. Zhang, and E. Yu, 2015: The impact of regional uplift of the Tibetan Plateau on the Asian monsoon climate. *Palaeogeogr. Palaeoclimatol. Palaeoecol.*, **417**, 137–150, <https://doi.org/10.1016/j.palaeo.2014.10.030>.